# Dating inset terraces and offset fans along the Dehshir Fault (Iran) combining cosmogenic and OSL methods

Kristell Le Dortz, Bertrand Meyer, Michel Sébrier, Regis Braucher, H. Nazari, L Benedetti, M. Fattahi, B. Bourlès, M. Foroutan, Lionel Siame, et al.

# Dating inset terraces and offset fans along the Dehshir fault combining cosmogenic and OSL methods

**K. Le Dortz [1,2], B. Meyer [1,2], M. Sébrier [1,2],R. Braucher [3], H. Nazari [4], L. Benedetti [3],M. Fattahi [5,6], D. Bourlès [3], M. Foroutan [4],L. Siame [3], A. Rashidi[7], and M. D. Bateman [6]**

1 - UPMC Univ Paris 06, ISTEP, UMR 7193, F-75005, Paris, France
2 - CNRS, ISTEP, UMR 7193; F-75005, Paris, France
3 - CEREGE UMR6635, Aix-En-provence, France
4- Research Institute for Earth Sciences, Geological Survey of Iran, PO Box 13185-1494 Tehran, Iran
5 - Institue of Geophysics, University of Tehran, Iran.
6 - Sheffield Centre for International Drylands Research, University of Sheffield, Sheffield S10 2TN, UK
7 - Geological Survey of Iran, PO Box 7615736841 Kerman, Iran

## Abstract

$^{10}$Be and $^{36}$Cl cosmic ray exposure (CRE) and optically stimulated luminescence (OSL) dating of offset terraces have been performed to constrain the long-term slip-rate of the Dehshir fault. Analysis of cosmogenic $^{10}$Be and $^{36}$Cl in 73 surface cobbles and 27 near-surface amalgams collected from inset terraces demonstrates the occurrence of a low denudation rate of 1 m.Ma$^{-1}$ and of a significant and variable inheritance from exposure prior to the aggradation of theses alluvial terraces. The significant concentrations of cosmogenic nuclides measured in the cobbles collected within the riverbeds correspond to 72 ± 20 ka of inheritance. The mean CRE age of the surface samples collected on the older terrace T3 is 469 ± 88 ka but the analysis of the distribution of $^{10}$Be concentration in the near-surface samples discard ages older than 412 ka. The mean CRE age of the surface samples collected on terrace T2 is 175 ± 62 ka but the $^{10}$Be depth profile discard ages older than 107 ka. For each terrace, there is a statistical outlier with a younger age of 49.9 ± 3.3 ka and 235.5 ± 35.4 ka on T2 and T3 respectively. The late sediments aggraded before the abandonment of T2 and inset levels, T1 b and T1a, yielded optically stimulated luminescence (OSL) ages of respectively 26.9 ± 1.3 ka, 21.9 ± 1.5 ka, and 10.0 ± 0.6 ka. For a given terrace, the OSL ages, where available, provide ages that are systematically younger than the CRE ages. These discrepancies between the CRE and OSL ages exemplify the variability of the inheritance and indicate the youngest cobble on a terrace, that minimizes the inheritance, is the most appropriate CRE age for approaching that of terrace abandonment. However, the upper bound

39 on the age of abandonment of a terrace that is young with respect to the amount of inheritance
40 is best estimated by the OSL dating of the terrace material. For such terraces, the CRE
41 measurements are complementary of OSL dating and can be used to unravel the complex
42 history of weathering and transport in the catchment of desert alluvial fans. This
43 comprehensive set of dating is combined with morphological offsets ranging from 12 ± 2 m to
44 380 ± 20 m to demonstrate the Dehshir fault slips at a rate in the range 0.9 $mm.yr^{-1}$ - 1.5
45 $mm.yr^{-1}$. The variable inheritance exemplified here may have significant implications for
46 CRE dating in arid endorheic plateaus such as Tibet and Altiplano.
47

## 1. Introduction

The Dehshir fault is a 380 km-long, strike-slip fault cutting through the Central Iran plateau, north of the Zagros. It is located between 29.5°N-54.6°E and 33°N-53.1°E and is part of a series of N-striking dextral faults slicing Central and Eastern Iran (e.g. Berberian, 1981). The total offset of the fault, denoted by the geological offsets of the Nain Baft suture and the Urumieh Doktar magmatic arc, amounts to 65 ± 15 km (Inset Figure 1; Walker and Jackson, 2004; Meyer et al., 2006). The southern portion of the Dehshir fault that runs across a series of Quaternary alluvial fans shows clear evidence of recent right-lateral motion (Figure 1). Geomorphologic studies have been performed to estimate the slip-rate of the fault. Combining cumulative offsets of gullies and terrace risers with their inferred Holocene age, Meyer et al (2006) and Meyer and Le Dortz (2007) suggested the fault slips at 2 $mm.yr^{-1}$. This initial estimate has been further investigated by dating of optically stimulated luminescence (OSL) samples collected within colluviums thought to predate the incision of an abandoned fan. Nazari et al (2009) derived a minimum slip-rate of 0.8-2.5 $mm.yr^{-1}$ by combining the offset of two gullies incised within the fan with the weighted mean OSL age of the colluviums. However, neither the offset-gullies nor the surface of the abandoned fan have been dated directly. Nazari et al. (2009) collected primarily the OSL samples for paleoseismic purpose, within the fault zone where fanglomerate layers have been disrupted and/or warped.

In order to date the surface of the fan and provide further constraints on the slip-rate, we have sampled the surface to estimate its cosmic ray exposure (CRE) age and the sediments below the surface for OSL dating of their emplacement. While these two dating techniques are commonly used separately, a few recent studies have combined luminescence dating with cosmogenic data. In some cases the two methods yielded comparable ages though the CRE ages are always slightly older than the OSL ones (e.g. Owen et al., 2003, 2006; De Long and Arnold, 2007). Other studies yielded to significant differences, CRE ages being as much as twice older than the OSL ones (Hetzel et al., 2004; Nissen et al., 2009; Le Dortz et al., 2009). Some authors favoured the CRE ages whether they used surface samples only (Hetzel et al., 2004) or near-surface samples only (Nissen et al., 2009). Others (Le Dortz et al., 2009) that used both surface and near-surface samples concluded to a variable inheritance for the CRE ages and favoured the OSL ages for dating the abandonment of alluvial surfaces.

We performed the sampling at two sites on the southern portion of the fault where Meyer et al. (2006) documented right-lateral offsets of imbricate fan surfaces and riser cuts (Figure 1). To constrain the age of the abandoned fan surfaces and the age of the subsequent

incision, we collected 100 samples (73 surface samples and 27 near-surface samples along three profiles) to determine their CRE age by measuring the accumulation of $^{10}Be$ and $^{36}Cl$ cosmogenic nuclides. Using two isotopes with markedly different half-lives offered the opportunity to better constrain the erosion rate and evaluate the trade-off between erosion and CRE age of the studied surfaces. We also collected six additional samples within quartz-rich sandy layers located below alluvial surfaces to measure by OSL the time elapsed since the last sunlight exposure of the sediment.

First, we describe the detailed morphology of the two sites with emphasis on inset terrace levels imbricate within successive alluvial fan systems. Then, we present the results of the CRE and OSL dating and discuss how far they help constraining the abandonment age of the terrace treads and the age of the riser cuts that bound the treads. Finally, we discuss the slip-rate of the Dehshir fault and the morphoclimatic chronology of the area.

## 2. Offset Quaternary fans along the southern portion of the Dehshir fault

### 2.1 Site Dehshir South: Marvast River

The Marvast River is the largest and the most active of the intermittent rivers draining the study area, a dryland part of endorheic Central Iran Plateau. The river course is about 70 km long from its source within the High Zagros to the South of the Marvast city. The incision of the Marvast River is limited because it vanishes into the Marvast salt flat, whose base level stands at the elevation of 1520m. The drainage basin of the Marvast River is about 1100 $km^2$, and the upstream catchment drains several distinctive rock units including cover (Zagros platform lithologies) and basement (Sanandaj Sirjan metamorphics). The river and its former tributaries have emplaced the vast Quaternary piedmont made of coalescent fans that cover most of the surface on the satellite imagery of figure 1. The recent incision of the piedmont has resulted in a narrow channel supplying water to the city of Marvast, the formation of inset terraces, and the fan head entrenchment. The Dehshir fault cuts across the Marvast River, the active fans and the abandoned fan systems (Figure 2). To the west of Marvast city, several inset terraces are distinguished (T0, T1a, T1b, T2, T3) and their relative age can be assessed by their relative elevation (Figure 3). The material of each terrace, well layered, is of fluvial-torrential origin and contains polygenic cobbles (Figure 3). The lower terrace T0 corresponds to the present-day overflowing flood channel of the Marvast River. Many braided channels up to 0.5-0.8 m deep incise T0. Very loose conglomerates alternate with silty-sandy layers. The pebbles and the cobbles, either in the riverbed or on the surface of T0 are well rounded and have not experienced cryoclasty. T1 is a terrace located 1 to 3 m above T0. T1 is made of two

114 distinctive levels, T1b slightly older and 1 m above T1a. Both T1a and T1b levels have been
115 probably emplaced during the same climatic period. They contain pebbles and well-rounded
116 cobbles with diameters up to 30 cm. The material is poorly cemented and some sandy layers
117 are found intercalated within the slightly indurate conglomeratic layers. Cobbles on the T1
118 surface display bar and swell morphology, most of them are well rounded very few have been
119 fragmented suggesting a very limited cryoclasty. T2 is an older terrace standing about 4-5 m
120 above T1 upstream of the Dehshir fault and 2-4 m above the present streambed downstream.
121 Several indurate sandy layers alternate with coarse conglomerates. T2 surface is flat and many
122 fragmented cobbles are found on it, suggesting that the terrace underwent low temperatures
123 and contrasted seasons during long period of times associated with strong wind deflation, as
124 under glacial climates. The upper part of the terrace is fairly cemented by a discontinuous
125 calcrete up to 1 m thick at some places. T3 is the top surface of the highest alluvial fan
126 system. It stands more than 5 m above T2. Where exposed upstream, by the Marvast incision,
127 T3 contains many cryoclasted cobbles and a few large cobbles. The conglomerate levels are
128 strongly indurate and the upper part of T3 is cemented by a continuous, 0.4-0.8 m thick,
129 reddish calcrete. Numerous gelifracted cobbles can be found on its surface. Many gullies
130 incise T3; they are deeper and wider than the shallow immature rills incising T2. The overall
131 terrace has a characteristic striped-morphology on the satellite imagery with flat strips
132 separated by narrow intervening intermittent gullies (Figure 2).
133 There are also a few remnants of older fanglomerates cropping out close to the fault
134 (Figure 2). These older conglomerates are assigned to the Pliocene according to the geological
135 mapping by GSI (1981). The layers are mostly tilted to the west and squeezed within the fault
136 zone, but the orientation of the cobbles indicates an eastward paleocurrent direction (Meyer et
137 al., 2006). The successive fans have been all emplaced by the Marvast River and
138 progressively deformed through time. The most recent riser cut of the Marvast river stands
139 between T1 tread and the river course (T1b/T0) West of the fault and between T2 tread and
140 the river course (T2/T0) East of the fault. This T2/T0 riser, deflected in a right-lateral sense
141 by an amount of 25 ± 5 m, is not a passive marker and might have been rejuvenated by lateral
142 erosion (Figure 2a). Several larger offsets occur further to the South. About 2 km south of the
143 Marvast River, a large dry river, deeply incised within the oldest fan T3, is right-laterally
144 offset by 380 ± 20 m (Figure 2b). This offset is higher than the 180-200m offset streams
145 described by Meyer et al. (2006) a little further to the South. The latter offsets correspond to
146 streams that are narrower and less incised than for the former. Consequently, the value of 380

± 20 m corresponds to the largest dextral offset observed amongst the many rivers incising T3 and provides a minimum bound of the fault motion since the abandonment of T3 tread.

## 2.2 Site Dehshir North

The site Dehshir North is located about 25 km north of the Marvast River (Figure 1). The site lies close to a 30 km long, north-south trending, intermittent stream in which present-day drainage is mostly restricted to the northern part of the piedmont. The stream is disconnected from the Marvast River but it grades almost back to the Marvast River outlet from the Sanandaj Sirjan Mountains and drains a significant area of the Quaternary piedmont. At site Dehshir North, the piedmont mainly consists of the distal part of the abandoned fan T3 (Figure 4). Similarly to the site Dehshir South, several lower levels (T2, T1b, T1a) with limited extension are nested within the alluvial fan T3. The material of each terrace is also of fluvial-torrential origin but the gravel sizes are smaller than at site Dehshir South. Fine content is higher and the coarser levels are void of boulders.

The higher level T3, although much resembling that along the Marvast River on the SPOT Imagery, has been a little less incised and dissected by the rivers than at Dehshir South. At Dehshir North, T3 stands about 4 m only above the active riverbed (Figure 4b) and its surface displays many cryoclasted cobbles. T3 is incised upstream by many short gullies regularly spaced every 20-30 m. Such gullies probably formed as a result of regressive erosion after the abandonment of the terrace T3 and the cutting of the risers. T2 has a very limited extension with respect to T3. It is a lateral fan sloping down gently northward that was aggraded by small local tributaries that are incised within T3 terrace and rework its alluvial material. T2 surface stands 2-4 m below T3 and is much less incised than the old terrace; only a few short gullies irregularly spaced are distinguished on the Quickbird Imagery (Figure 4a). As T3, the surface of T2 displays cryoclastic material. The emplacement of the lateral fan T2 is partly controlled by the local development of the Dehshir fault. The terrace T1 lies 1 m at most below the terrace T2 and stands 1 m above the riverbed T0. Most of the gullies that incise T3 and T2 merge downstream with T1 and their incision is probably synchronous with the emplacement of T1. The surface of T1 displays only very few cryoclasted cobbles. Similarly to the site Dehshir South, two levels (T1a and T1b) can be distinguished, with T1b being older and standing 0.5-1 m above T1a. Both the terrace T1 and the lateral fan T2 are nested in the highest terrace T3 and have a very limited extent.

Some small gullies that incise T3 and T2 cross the fault zone at a right angle. Two of these gullies are clearly offset in a right-lateral sense by 20-30 m (figure 4), an amount similar

to the deflection of the Marvast River at the site Dehshir South. These gullies postdate the emplacement of T3 and T2 and might have formed as a result of regressive erosion since the last significant incision of the network. Their incision is probably coeval with the emplacement of the terrace T1 with which they merge downstream, and the gullies, according to weighted mean OSL dating in a trench within the fault zone, are supposed to be younger than 21.1 ± 11.2 ka (Nazari et al., 2009). There is also an offset of the right bank of the main river flood channel (Figure 5). Upstream, the most recent riser cut (T3/T0) stands between T3 tread and the riverbed. Downstream, T1 is protected from erosion because of the right-lateral motion of the fault and the most recent riser stands between T1 tread and the riverbed (T1a/T0). The riser that postdates the terrace T1a is offset by 12 ± 2 m (Figure 5).

## 3. Chronology of the regional fans

The dating of the alluvial surfaces and inset terraces at both sites is required to establish the chronology of the fans and constrain the age of the offset-risers. Two complementary dating methods, cosmic ray exposure (CRE) and optically stimulated luminescence (OSL), have been performed to estimate the age of abandonment of alluvial surfaces. OSL relies on natural background radioactivity of the material with a small contribution of cosmogenic radiation and measures the time elapsed since the last sunlight exposure of a sediment layer. CRE provides the time of exposure of superficial material to cosmic rays.

### 3.1 Sampling strategy and analytical procedures for cosmogenic and OSL dating

All the terraces (T0, T1, T2 and T3) were sampled at each site for cosmogenic dating. For some surfaces (T3 at sites Dehshir North and Dehshir South, T2 at site Dehshir South) and taking advantage of the occurrence of polygenic cobbles, both the $^{10}$Be and $^{36}$Cl cosmogenic nuclides dating techniques have been applied. We measured the concentrations of *in-situ* produced $^{10}$Be and $^{36}$Cl accumulated respectively in quartz-rich and carbonates samples exposed to cosmic rays. Surface samples were collected to estimate the CRE ages (Table 1). Most of the surface samples, 67 over the 73 collected, consists of individual cobbles, 4 correspond to two fragments of the same gelifracted cobble, and 2 only are amalgams of many (about 25) pieces of small pebbles. Near-surface samples were also collected along three profiles to estimate the inheritance, i.e., the concentrations of cosmogenic nuclides accumulated in the cobbles prior to their deposition. Each near-surface sample is an amalgam of pebbles or fragments of cobbles collected at the same depth. Provided that the sediment emplaced in a short period of time and that the pre-exposure is homogeneous, the exponential

decrease of concentrations with depth provides an estimate of the homogeneous inheritance (e.g. Anderson et al., 1996; Repka et al., 1997). The inherited concentration is determined from the asymptotic value that the profile tends to at depth and a chi-square inversion is often used to minimise the differences between measured and modelled concentrations (e.g., Siame et al., 2004; Braucher et al., 2009). Collecting pebbles from the active streambed also helps to estimate the inherited component (e.g. Brown et al., 1998). However, this method relies on the questionable assumption that the pre-depositional history of the pebbles collected in the present-day streambed is comparable to that of the pebbles collected on abandoned fan surfaces during aggradation stages.

Three main types of secondary particles are involved in the *in situ* production of $^{10}$Be: fast nucleons (essentially neutrons), stopping (or negative) muons and fast muons. Each of them has its own effective attenuation length. We used in this paper the same parameters as Braucher *et al*. (2003) for the muonic attenuation lengths that are 1500 g.cm$^{-2}$ for stopping muons and 5300 g.cm$^{-2}$ for fast muons. For fast neutron, an attenuation length of 160 g.cm$^{-2}$ (Gosse and Phillips, 2001) is used rather than the attenuation length of 177 g.cm$^{-2}$ (Farber et al., 2008) modelled at mid-lattitude in California but without accounting for the muonic contribution. Samples were prepared at the CEREGE laboratory in Aix-en-Provence for $^{10}$Be concentration measurements following chemical procedures adapted from Brown et al. (1991) and Merchel and Herpers (1999). After addition in each sample of ~100 $\mu$l of an in-house 3.10$^{-3}$ g/g $^{9}$Be carrier solution prepared from deep-mined phenakite (Merchel et al., 2008), all $^{10}$Be concentrations were normalized to $^{10}$Be/$^{9}$Be SRM 4325 NIST standard with an assigned value of (2.79 ± 0.03).10$^{-11}$. This standardization is equivalent to 07KNSTD within rounding error. All $^{10}$Be data reported in this study (Table 1) have been measured at ASTER (CEREGE, Aix-en-Provence). Analytical uncertainties (reported as 1σ) include uncertainties associated with AMS counting statistics, AMS external error (0.5%), chemical blank measurement. Long term measurements of chemically processed blank yield ratios on the order of (3.0 ± 1.5).10$^{-15}$ (Arnold et al., 2010). Cosmocalc add-in for excel (Vermeesch, 2007) has been used to calculate sample scaling and standard atmospheric pressures. Stone (2000) polynomial has been used to determine surficial production rate assuming a SLHL production rate of 4.49 at.g$^{-1}$.yr$^{-1}$ for $^{10}$Be.

$^{36}$Cl can be produced by two mechanisms in superficial rocks, cosmic ray interactions (spallation reactions of Ca, K, Ti and Fe, capture of low energy epithermal and thermal neutrons by $^{35}$Cl, and direct capture of slow negative muons by K and Ca) and radiogenic production by disintegration of U and Th. To determine the proportion of radiogenic $^{36}$Cl requires measuring the concentrations of U and Th in the target mineral (Zreda et al., 1991; Stone et al., 1996, 1998; Gosse & Phillips 2001; Schimmelpfennig et al., 2009). Major elemental compositions of rock samples were determined by ICP-OES technique by the CNRS service for rocks and minerals analysis at CRPG Nancy. For the $^{36}$Cl measurements, the chemical extraction of chlorine by precipitation of silver chloride has been adapted from the protocol of Stone et al. (1996). The samples were spiked with a known quantity of stable chlorine carrier (e.g. Desilets et al., 2006) to simultaneously determine $^{36}$Cl and chlorine concentrations by isotope dilution accelerator mass spectrometry (AMS). The chemical treatment of the samples was carried out at the CEREGE laboratory in Aix-en-Provence and the measurements were performed at the Lawrence Livermore National Laboratory, using KNSTD1600 standard. The excel spreadsheet provided by Schimmelpfennig et al., (2009) was used to calculate all $^{36}$Cl production rates and to model $^{36}$Cl data. Accordingly, a surface spallation rate of 48.8 ± 3.4 at.g$^{-1}$(Ca).yr$^{-1}$ (Stone et al. 1996) is used. However we use a neutron attenuation length of 160 g.cm$^{-2}$ (Gosse & Phillips 2001) instead of 177 g.cm$^{-2}$ (Farber et al., 2008) as explained above and for self consistency. The concentrations of *in-situ* produced $^{10}$Be and $^{36}$Cl are given in Table 1 and the chemical composition of the carbonate samples in Table 2.

Optically stimulated luminescence was used to date the alluvial layers emplaced during the aggradation of the fans. Lenses of fine sandy-silts intercalated between conglomerates at various depths below the surface were sampled for OSL in opaque tubes. The Single Aliquot Regeneration (SAR) protocol (e.g.; Murray and Wintle, 2000) was employed for the Equivalent dose (De) measurement once quartz had been extracted and cleaned from each sample. The analytical procedures employed are identical to that applied to similar samples from the neighbouring Anar, Sabzevar and Doruneh areas (Le Dortz et al., 2009; Fattahi et al, 2006; 2007).

Initial attempts to use single grains for De determination failed due to the dimness of OSL signal. As a result De measurements were undertaken on 9.6 mm diameter aliquots containing approximately 1500-2000 grains. Whilst normally this might result in averaging

out of any multiple dose component within a sample, here it is assumed that for these dim samples the luminescence signal from each aliquot was produced by a relatively few number of bright grains and thus may be considered as almost measuring at single grain level. Therefore, the De distribution of the single aliquot De measurements is considered to be almost a true reflection of the actual De distribution within a sample. For some samples the depositional setting, field sedimentary logs and the scatter of the replicate aliquot De data indicated that prior to burial, full resetting (bleaching) of the OSL signal had not taken place and/or that the sediments had undergone some post-depositional disturbance (Bateman et al., 2007). As a result of this, Finite Mixture Model (FMM; Roberts et al. 2000) was used where samples showed skewed, scattered, or multimodal distributions. We used the dominant FMM component for samples displaying multimodal De distributions and the lowest FMM component of De for samples whose De distributions were skewed (assuming partially bleached without significant bioturbation) samples (Boulter et al., 2007; Bateman et al., 2007). Where samples had a low over-dispersion and unimodal, normally distributed De's then the Central Age Model (CAM; Galbraith et al., 1999) De was used for age calculation purposes. The relevant information for OSL ages are presented in Table 3 in years from present with 1 sigma errors.

## 3.2 Cosmic ray exposure ages

Figure 6 displays the results for the site Dehshir North, and figure 7 for the site Dehshir South. The concentrations are given in Table 1 with the corresponding CRE ages modelled assuming erosion and inheritance are negligible.

### 3.2.1 Surface T3

For T3, both the $^{10}$Be and $^{36}$Cl zero-erosion, zero-inheritance ages of surface samples are overall consistent and suggest that the terrace tread is old.

At Dehshir North (Figure 6), the CRE ages range between 235 and 519 ka for the $^{10}$Be measurements, and between 268 and 383 ka for the $^{36}$Cl measurements. For the $^{10}$Be concentrations, all but one surface sample provide CRE ages greater than 400 ka. The younger $^{10}$Be exposure age (DN06S2, 235.5 ± 35.4 ka) might be considered as an outlier and excluded from the statistics. Then, the weighted mean of the zero-erosion zero-inheritance $^{10}$Be model age of T3 is 462 ± 55 ka while the $^{36}$Cl one is 325 ± 74 ka (Figure 6b).

At site Dehshir South (Figure 7), the scattering of the concentrations is greater. The weighted means of the zero-erosion zero-inheritance $^{10}$Be and $^{36}$Cl ages are 481 ± 119 and 344 ± 83 ka, respectively (Figure 7b). The results are nonetheless similar at both sites and confirm the qualitative inference of the synchronism of levels T3 drawn from the resemblance of their surface at distant sites on the Quickbird imagery. They indicate T3 is a rather old surface (several hundreds ka) and that $^{36}$Cl surface ages are a little younger than $^{10}$Be ages. The slight difference between the $^{10}$Be and $^{36}$Cl weighted mean ages may either result from a statistical bias due to the limited number of samples or be meaningful. The $^{36}$Cl half-life (301 ka, e.g. Gosse & Philipps, 2001) being lower than that of $^{10}$Be (1.387 ± 0.12 Ma, Chmeleff et al., 2009; Korshinek et al., 2009) and T3 an old terrace, the difference may suggest the carbonates have reached the steady-state equilibrium for which the production of $^{36}$Cl is balanced by the loss due to radioactive decay and the loss due to erosion, if there is any.

Because there is a trade-off between denudation rate and exposure age, it is important to estimate the erosion. Assuming an infinite age for the emplacement of T3 allows estimating a maximum erosion rate for each of the surface samples, both for $^{36}$Cl and $^{10}$Be isotopes (Table 1). For the carbonates, none of the surface samples provides a $^{36}$Cl maximum denudation rate greater than 2.1 m.Ma$^{-1}$, and the averaged value is 1.5 m.Ma$^{-1}$. Discarding the outlier DN06S2, the quartz surface samples indicate a $^{10}$Be maximum denudation rate smaller than 1.6 m.Ma$^{-1}$ with an averaged value of 1.4 m.Ma$^{-1}$. This is further strengthened by modelling the depth-distribution of the $^{36}$Cl concentrations in the amalgamated carbonate samples collected along a 3 m depth profile excavated in T3 at the site Dehshir North (Figure 8). The profile shows an overall exponential decrease of concentrations with depth allowing for modelling the erosion rate. The $^{36}$Cl concentration depth profile is modelled with assigning a surface age of 3 Ma; old enough to ascertain the equilibrium between production and disintegration has been reached. Letting the erosion rate and the inheritance free to vary, the profile is modelled for three density values (between 2 and 2.4 g.cm$^{-3}$) within the range of that measured for the samples of the profile (Figure 8). For all the densities tested, the model converges towards zero inheritance solutions and low erosion rates. The solutions with zero inheritance are not surprising because the assigned surface age of 3 Ma makes a homogeneous inheritance of several tens of ka undetectable. By contrast, the solutions with low maximum erosion rates are meaningful. The greatest erosion rate of 1.90 m.Ma$^{-1}$ is obtained for a density value of 2 g.cm$^{-3}$. Smaller erosion rates of 1.48 and 1.18 m.Ma$^{-1}$ corresponding to densities of 2.2 and 2.4

346 g.cm$^{-3}$are closer to the erosion rate calculated for each of the carbonate surface samples (Table
347 1).

348 Whatever the method applied (surface sample, near-surface samples and depth-profile
349 modelling) and whatever the isotope considered, the estimates of the maximum erosion rate
350 are very low. They are close to that found in hyperarid regions (<1 m.Ma$^{-1}$, Matmon et al.,
351 2009) and in good agreement with the pristine morphology of the flat-topped surface of T3.
352 The $^{10}$Be depth profile can be theoretically modelled with erosion rates ranging between 0 and
353 1.4 m.Ma$^{-1}$, maximum erosion rate averaged from the $^{10}$Be surface samples. Accounting for
354 the trade-off between erosion rate and exposure age (the higher the erosion rate, the older the
355 exposure age), the $^{10}$Be depth profile has been modelled under the assumption of no erosion to
356 minimize the exposure age. We hence tested a range of inheritance values to solve for the zero
357 erosion exposure age (Figure 9). The best fit is obtained for a surface age of 464 ka and a
358 homogeneous inheritance of 3.8 $10^5$ at.g$^{-1}$($SiO_2$). This inheritance, if acquired at the surface
359 and prior to the emplacement of the terrace, would correspond to a period of pre exposure of
360 about 32 ka, small with respect to the exposure age. Accounting for the trade-off between
361 inheritance and age, several other solutions remain acceptable (Figure 9b). Assuming a
362 homogeneous inherited concentration of 7.6 $10^5$ at.g$^{-1}$($SiO_2$), twice that obtained for the best
363 fit and close to the concentration measured for the deepest sample of the profile, provides an
364 age of 327 ka. Hypothesizing zero inheritance yields an older age of 686 ka that does not
365 match with the concentrations of surface samples, demonstrating the usefulness of combining
366 both surface and near-surface sampling.

367 In summary, T3 is a rather old and well-preserved alluvial surface, in which cobbles
368 have incorporated a poorly constrained inheritance of several tens of ka. This amount of
369 inheritance, though limited with respect to the CRE age of T3, contributes to the 469 ± 88 ka
370 weighted mean age of all the quartz cobbles collected on the terrace tread at sites Dehshir
371 North and Dehshir South (Figure 10).

372

373 3.2.2 Surface T2

374 At Dehshir North, only one amalgam quartz-rich surface sample has been dated on T2
375 fan surface. The zero-erosion zero-inheritance CRE age is 406.5 ± 26.5 ka (Table 1, Figure
376 6a). This age is a little younger than of the weighted mean age of T3 and agrees with the
377 assumption that T2 aggradation at this site results from reworking of T3 material. Indeed, T2
378 CRE age is older than several ages that have been used to estimate the weighted mean age of
379 T3 and much older than that of the T3 outlier. At Dehshir South, twelve samples collected on

T2 have been analysed (Figure 2a and Figure 7). The $^{10}$Be and $^{36}$Cl concentrations, hence the corresponding CRE ages calculated assuming zero-erosion and zero-inheritance are scattered (Table 1, Figure 7a). The CRE ages of the surface samples range between 49.9 ± 3.3 and 225.8 ± 14.7 ka for the $^{10}$Be and between 104.4 ± 10.5 and 190.3 ± 20.8 ka for the $^{36}$Cl. The youngest $^{10}$Be CRE age on T2 (DS08S114, 49.9 ± 3.3 ka) might be considered as an outlier and excluded from the statistics. Discarding the outlier and keeping in mind the limited number of samples, the ages remain scattered without significant differences between $^{10}$Be and $^{36}$Cl ages. The distribution is multimodal with a weighted mean CRE age of 175 ± 62 ka (Figure 11a). This average is consistent with the intermediate elevation of T2 terrace and its surface characteristics as well as the fact that none of the CRE ages obtained for T2 is older than the youngest age calculated for T3.

Amalgamated samples have also been collected along two depth profiles at site Dehshir South. The $^{10}$Be concentrations are listed in Table 1. The profile PS1 was collected by the riser between T2 and the Marvast riverbed, 300 meters East of the fault zone (Figures 2 and 11). The profile PS2 has been collected 1.5 kilometres NE of PS1, close to the fault scarp in a pit dug within the T2 surface and nearby remnants of T3 (Figures 2 and 12). For both profiles, the uneven distribution of the $^{10}$Be concentrations dismisses a uniform pre-exposure prior to the emplacement of T2 material and precludes any appropriate modelling of a homogeneous inheritance. As for the study of alluvial surfaces in the Anar neighbouring area (Le Dortz et al., 2009), the profile data, together with the scattering of the concentrations of the surface cobbles, suggest the occurrence of a variable inheritance.

### 3.2.3 Surface T1 and T0

At site Dehshir North, the four surface samples collected on T1a provide CRE ages ranging between 82 and 424 ka (Figures 4 and 6a). The sample with the oldest age might be considered an outlier and the CRE age of the terrace would be better determined by the three youngest samples and bracketed between 82 and 134 ka. The T1a outlier has an age close to that of the amalgam on T2 fan surface and close to that of the surface samples collected on T3. This suggests that the T1a outlier is a T2 or T3 cobble reworked by the small gullies incising the surface of T2 and T3 treads and which incision is coeval with the emplacement of T1.

At site Dehshir South, the four surface samples have been collected on T1b. They provide $^{10}$Be exposure ages ranging between 30 and 318 ka (Figures 2 and 7a). The oldest sample, even older than the samples collected on T2 tread, is as an outlier. Either it is a

former cobble of T3 locally reworked by the small gullies incising T3 or a cobble exposed to cosmic rays for a long time in the upstream catchment of the Marvast River. In any case, such an outlier indicates that the inheritance of individual cobbles collected on T1 tread can be very important. Off the three remaining samples collected on T1b, two provide CRE ages that are not distinguishable from the CRE weighted mean age (175 ± 62 ka) of T2, the terrace immediately above. Only one sample (DS08S124, 32.1 ± 2.1 ka) provides an age significantly younger than the ages on T2. This CRE age on T1b surface is significantly younger than the CRE ages on the T1a surface at site Dehshir North, suggesting that at this latter location, the surface cobbles of the T1a terrace contain an important amount of inherited $^{10}$Be.

At site Dehshir South, five samples have been collected in the present day streambed of the Marvast River. Whatever the isotope considered, all provide non-zero CRE ages ranging between 54 and 96 ka, suggesting the occurrence of a significant inheritance. The CRE ages of T0 are younger than the CRE ages of T1b except for the youngest sample of T1b (DS08S124, 32.1 ± 2.1 ka). At site Dehshir North, four samples have been collected in the main river flood plain T0. Discarding the outlier, three samples (two $^{10}$Be ages and one $^{36}$Cl age) provide non-zero CRE ages ranging between 57 and 84 ka, confirming the occurrence of a significant inheritance averaging some 70 ka. When including the outlier corresponding to the oldest sample collected in the river, the scattering of the concentrations increases and suggests the pre exposure history of a cobble before the abandonment of an alluvial surface is highly variable.

To summarize (Figure 13a), the observed average inheritance in the present stream beds of some 70 ka, as well as the distribution of CRE ages for the inset levels T1 and T2, suggest that T1 and T2 treads are likely to be younger than their CRE weighted mean age. Thus, the ages of abandonment of the terrace treads may be better approximated by the CRE age of the youngest sample found on each surface. Such a conclusion has already been drawn for alluvial fan surfaces in the neighbouring region of Anar (Le Dortz et al., 2009).

### 3.3 Optically stimulated luminescence ages

OSL dating was performed to better constrain the chronology of alluvial terraces at the two studied sites. Five OSL samples initially sought to determine the ages of faulted deposits for paleoseismology purposes were sampled at site Dehshir North (Nazari et al., 2009). Then, six new OSL samples were collected at site Dehshir South. As no suitable material was found within old terrace T3, OSL ages help only constraining the aggradation timing of terraces T2

448 and T1; they also permit comparison with CRE ages. The ages of all the OSL samples,
449 including those previously published by Nazari et al. (2009), have been recalculated in section
450 3.1 using CAM or FMM techniques to account for the scatter of the De distributions.
451 OSL samples were collected at site Dehshir North, in a trench excavated within T3
452 and T2 (Figure 4 in Nazari et al., 2009). Within this trench, the distal alluvial and colluvial
453 deposits corresponding to the T2 and subsequent levels provide refined OSL ages of 60.0 ±
454 5.7 ka, 45.5 ± 4.6 ka, and 20.1 ± 1.6 in accord with the stratigraphic succession (Table 3,
455 sample HI/2008-IX in unit E1, sample HI/2008-VII in unit D3b, sample HI/2008-VIII in unit
456 D4, Nazari et al., 2009). In addition, recent colluviums incised by small streams flowing
457 through the Dehshir fault zone and which base level matches with the tread of T1 yielded two
458 OSL ages of 26.0 ± 1.0 ka for the lower colluviums and 20.2 ± 0.8 for the upper ones (Table
459 3, sample HI/2008-I in unit B1 and sample HI/2008-VI in unit B2, Fattahi et al., 2010). These
460 two latter OSL ages, which postdate the incision of T2, are coeval with the emplacement of
461 T1. They imply that the T1b tread, all the more the T1a tread, is at most 21 ka (oldest possible
462 age of the most superficial sample). Notwithstanding that the OSL samples have not been
463 directly collected under the terrace treads sampled for CRE dating, the data available at site
464 Dehshir North indicate large discrepancies between the CRE and OSL ages. The cannibalism
465 of the old T3 terrace by subsequent alluvial deposits may explain such discrepancies by
466 locally recycling T3 cobbles during the aggradation of the lower terraces T2 and T1. This
467 possibility is further examined at site Dehshir South for which OSL samples have been taken
468 right below the terrace treads T2 and T1 where sampled for CRE dating.
469 For T2 at Dehshir South, two OSL samples, OSL I and OSL II, have been collected
470 from the riser between T2 and the active riverbed, very close to the profile PS1 (Figure 2a and
471 11b). OSL I has been collected 15 m to the West of PS1 and at a depth of 0.8 (OSL I) and
472 OSL II, 10 m to the East of PS1 and at a depth of 3.4 m. The samples OSL I and II yielded
473 ages of 26.9 ± 1.3 ka and 29.4 ± 5.1 ka, respectively (Table 3). These similar OSL ages
474 suggest that the material of the terrace T2 emplaced rapidly and that its tread is at most 28.2
475 ka. The OSL samples of the riser T2/T0 provide ages much younger than the weighted mean
476 $^{10}$Be and $^{36}$Cl CRE age of T2, 175 ± 62 ka (Figure 11a), but closer to 49.9 ± 3.3 ka, the
477 youngest CRE age on T2 tread (DS08S114 in Table 1). Two additional OSL samples
478 (AB/2006-I and II in Table 3) were collected within a colluvium pediment topping T2 in the
479 pit of profile PS2 (Figure 2a and 12b). These samples yielded OSL ages of 39.7 ± 2.6 and
480 20.0 ± 1.3 which confirm this desert pediment was formed both by the end of the
481 emplacement of terrace T2 and after its abandonment. To summarize, the OSL ages obtained

for T2 indicate its aggradation occurred during the time-interval 25.6-65.7 ka. This suggest that the samples collected on T2 tread, providing exposure ages older than 66 ka, contain an inherited CRE component, For T1, two OSL samples, OSL III and IV, were collected at Dehshir South in fine sands respectively below the surface of T1b and T1a (Figure 3b). The error bars on sample OSL III, taken by the riser T1b/T0, provide minimum and maximum OSL ages of 20.4 ka and 23.4 ka for the T1b tread. The sample OSL IV, taken by the riser T1a/T0, provides minimum and maximum OSL ages of 9.4 ka and 10.6 ka for the T1a tread. These ages are in agreement with the relative elevation of the terraces, the samples from the riser T2/T0 being older than the sample from the riser T1b/T0, itself older than the sample from the riser T1a/T0. Similarly to the terrace T2, the OSL age of T1b is younger than the $^{10}$Be CRE ages of the samples collected on the T1b tread. This OSL age is almost one order of magnitude younger than the three oldest $^{10}$Be samples and 30% younger than the youngest $^{10}$Be sample (DS08S114). There is no direct comparison available between OSL and CRE ages for T1a because this surface has not been sampled for cosmogenic dating.

At the two studied sites along the Dehshir fault, the OSL ages on terraces T2 and T1 are systematically younger than the CRE ones on the same terrace. For a given terrace, the CRE statistical outlier, which is the youngest CRE age and has been consequently removed from the calculation of the weighted mean CRE age, remains slightly older than, but closer to the OSL ages. Two extreme options may be contemplated: either OSL ages have been rejuvenated or CRE concentrations include a high percentage of inheritance. Most of the physical processes that are known to affect the OSL method, such as partial bleaching, incorporate an antecedent signal leading to overestimation of the age of sediment burial. This has been accounted for the studied samples by the statistical processing of the De distributions. Conversely, OSL signal is sensitive to the temperature and a loss of luminescence might occur at temperatures above 50°- 60°C. Such temperatures may occur on the Iran plateau during summertime so that OSL ages could be theoretically rejuvenated. Nevertheless, to account for gamma rays shielding, OSL samples were taken at least at 0.7 m below the ground surface (Table 3), a depth large enough to prevent strong variations of temperature. In addition, if temperature had affected the OSL signal, such effect would decrease with increasing sampling depth. However, no trade-off is observed between the OSL ages and the sampling depth (Table 3). On the contrary, OSL ages, whatever the depth, appear similar for the same terrace and in agreement with the relative elevation of the terraces. As a consequence, the variable inheritance of CRE concentrations should chiefly explain the discrepancy with OSL ages.

516

517 **3.4 Discussion on the abandonment age of the alluvial surfaces**

518 The overall chronology of the fan surfaces crossed by the Dehshir fault has
519 been established but the abandonment age of each surface is not easily assigned for several
520 reasons (Figure 13). First, the scattering of CRE concentrations on a given surface, the
521 occurrence of more concentrated samples on younger surfaces than on older ones, the
522 occurrence of significant concentrations in active river beds, indicate there is a variable
523 inheritance uneasy to account for. Second, where CRE and OSL data are available for the
524 same terrace, the OSL ages of the late sediments of the terrace are always much younger than
525 the CRE ages of the cobbles abandoned on its tread. Such disparities between OSL and CRE
526 ages appear to result from the high variability of the CRE inheritance that needs further
527 consideration.

528

529 3.4.1 Variable CRE inheritance and maximum abandonment ages of alluvial treads.
530 A rough estimate of the variable inheritance is provided by the CRE weighted mean of 72 ±
531 20 ka obtained from 8 of the 9 samples collected in the riverbeds once the oldest outlier
532 discarded. Moreover, amalgam sample DS08P130 from profile PS1 (Figure 11c) has a
533 measured concentration (Table 1) of 8.86 $10^5$ at.$g^{-1}$($SiO_2$), even though it is located at 2.1 m
534 below the T2 surface whose surface samples yielded a weighted mean CRE age of 175 ±
535 62 ka. Assuming 175 ka represents the actual age of T2 tread and subtracting the
536 concentration acquired *in situ*, at 2.1 m depth, by sample DS08P130 during these 175 ka of
537 exposure would yield to a remaining, hence inherited, concentration of 7.25 $10^5$ at.$g^{-1}$($SiO_2$).
538 Most of the sample concentration would therefore result from inheritance. Such inherited
539 concentration would have been acquired in about 60 ka, if accumulated at the surface. Then,
540 the 70 ka ages of riverbed samples appear to give a good estimate of the amount of
541 inheritance carried by T2 material. Consequently, T2 mean age should be reduced to 105 ±
542 62 ka. These 70 ka inheritance estimates are larger than the 32 ka of inheritance age-
543 equivalent obtained for T3 by conventional modelling of the $^{10}$Be profile (Figure 9). We have
544 therefore investigated another method to use the inheritance. Assuming each terrace formed
545 during a short-lived aggradation coeval with a single climatic crisis, the near-surface
546 concentrations have been used to fix the maximum abandonment age of the terrace (Figure
547 14). The principle is simple and rests on the impossibility for any sample to be incorporated
548 into the sediment of the terrace with a negative concentration. Accounting for the depth of
549 each near-surface sample and assuming its measured concentration results only from *in-situ*

exposure; i.e. assuming no inheritance for the sample, it is possible to calculate for any sample of a profile the time required to bring it back from its measured concentration to a null concentration. The maximum abandonment age of the terrace is then obtained from the near-surface sample of a given profile for which the concentration is restored to zero without bringing back any other sample of the profile to a negative concentration. For the profile PS1 across T2 (Figure 14a), this is obtained for the sample DS08P127 with 107 ka of *in-situ* exposure. This indicates that T2 was abandoned at most 107 ka ago and that for this maximum time of exposure the concentration remaining in the other samples of the profile correspond to a minimum inheritance. Therefore, this method figures out the variability of the inheritance that amounts, for such an exposure time, to 7.86 $10^5$ at.$g^{-1}$($SiO_2$) for the near-surface amalgam collected at 2.1 m depth; such concentration would correspond to a minimum exposure of 66 ka if acquired at the surface prior to the emplacement of the terrace (Figure 14a). It is worth noticing that this rejuvenation would bring back only one of the surface samples to a negative concentration. This remains acceptable, as this sample is the statistical outlier DS08S114. All the other such 107 ka-rejuvenated surface samples would keep positive concentrations. While older depth-profile determined CRE ages of T2 are not possible because they would bring, at least one of the near-surface amalgams, the amalgam 127 (Figure 14a), back to a negative concentration, younger exposure ages remain possible. Theoretically, all exposure ages ranging between 0 and 107 ka are possible. On the one hand, exposure ages ranging between 53 ka (oldest possible age of the youngest sample, DS08S114, on T2) and 107 ka would make that statistical outlier younger than the age of the terrace. On the other hand, exposure ages ranging between zero and 53 ka would be compatible with the occurrence of the statistical outlier as well as the other surface samples collected on T2.

The same method applied to the depth profile PN across T3 (Figure 14b) demonstrates the terrace was abandoned at most 412 ka ago, confirms the occurrence of a significant inheritance which minimum amounts to 68 ka for the deepest amalgam collected at more than 3m depth, and exemplifies its variability. It is nonetheless important to notice that this is an uppermost bound of exposure duration. This leaves open all the possibilities ranging between the time of abandonment of T2 and 412 ka, hence at least the possibilities between 107 and 412ka.

### 3.4.2 Abandonment age of terrace treads.

The age of abandonment of the uppermost level T3 is to be discussed with the only data available, the CRE ages (Figures 13 and 15). One may rest on the statistical analysis of

584 the surface samples and retains the weighted mean age of 469 ± 88 ka. To account for the
585 inheritance incorporated in the former estimate, it is possible to subtract to that weighted
586 mean age the 32 ka of inheritance age-equivalent obtained from the modelling of the $^{10}Be$
587 profile. It is nonetheless worth noticing that this average inheritance has been modelled under
588 the incorrect assumption that the inheritance is homogeneous. Accounting for the variability
589 of the inheritance, the near-surface profile data are incompatible with an age older than 412 ka
590 (Figure 14b) and the large uncertainties of the former estimate (437 ± 88 ka) can be reduced
591 to the interval 349-412 ka (Figure 15). Alternatively, retaining the youngest sample and
592 allowing for the occurrence of a greater amount of inheritance would provide a much younger
593 abandonment age of 271 ka (oldest possible CRE age of the youngest sample). As there is
594 ample evidence for a large variability of the inheritance on the younger surfaces, one cannot
595 rule out the later hypothesis and may consider an age of 271 ka for the abandonment of T3.
596 The age of abandonment of the intermediate level T2 is easier to estimate because both
597 OSL and CRE ages are available. The weighted mean of the zero-erosion CRE age (175 ± 62
598 ka) is of little use for constraining the age of abandonment because of the variable inheritance.
599 Subtracting a possible inheritance of 70 ka (Figure 14a), a value similar to the average
600 obtained for the cobbles collected in the active riverbed, takes back the former estimate to 105
601 ± 62 ka. Although limiting the uncertainties to the range 43 -107 ka, the upper bound on the
602 abandonment age (Figure 14a) allows for a wide range of possibilities, including the oldest
603 possible CRE age (53 ka) of the youngest surface cobble. Accounting for the occurrence of a
604 variable inheritance, this latter solution is a better estimate of the maximum age of
605 abandonment of the surface although the youngest cobble may also bear an inherited
606 component. This inherited component may correspond to the difference with the oldest
607 possible age of the youngest OSL collected below the tread of T2. The surface of T2 is
608 younger than the oldest possible age of the superficial OSL sample and is at most 28.2 ka at
609 site Dehshir South (Figure 13b). Assuming this OSL age is close to the actual abandonment
610 age of T2 tread, a forward modelling of near-surface concentrations of PS1 profile (fig 11c)
611 can be calculated with zero erosion and different choices of inheritance. Whatever the
612 selected value of homogeneous inheritance, none permits to account correctly for the uneven
613 distribution with depth of the measured near-surface concentrations. Nevertheless, two
614 limiting curves appear to bracket these measured concentrations, they correspond to 3.5 $10^5$
615 and 9 $10^5$ at.$g^{-1}$($SiO_2$) of homogeneous inheritances (figure 11c). These values of inherited
616 concentrations would correspond to pre-exposure, if acquired at the surface prior to the
617 emplacement of the terrace, of 30 ka and 75 ka, respectively. Although these values of

inherited concentrations result from forward modelling based on the assumption that the inheritance is homogeneous, they indicate the inheritances carried by the amalgam samples of T2 sediments may be nearly as high as $10^6$ at.g$^{-1}$($SiO_2$). It is worth noticing that all but one measured surface samples have $^{10}$Be concentrations that are higher than $10^6$ at.g$^{-1}$($SiO_2$). Interestingly, subtracting to the near-surface samples the concentrations corresponding to 30 ka of *in-situ* exposure makes the residual concentrations, which correspond to inheritance, noteworthy. This inherited concentration amounts to 8.57 $10^5$ at.g$^{-1}$($SiO_2$) for sample DS08P130 at 2.1 m depth and corresponds to pre-exposure time at the surface of 71 ka. Thus considering 70 ka of inheritance for T2 gravels is a reasonable estimate that can be proposed to average the variable inheritance.

Finally, the OSL ages of the risers T1b/T0 and T1a/T0 indicates their respective tread are at most 23.4 ka and 10.6 ka, respectively. Given the uncertainties associated to the OSL ages of the risers and considering that partial bleaching has been accounted, the youngest possible ages of T2, T1b, and T1a treads are respectively 25.6 ka, 20.4 ka, and 9.4 ka.

## 4. Slip-rate estimate and conclusions

The former chronology and offset-risers provide estimates on the minimum and maximum slip-rate of the Dehshir fault. At site Dehshir South, the river course displaced by 380 ± 20 m is incised within the terrace T3. Combining the offset of 380 ± 20 m with the maximum exposure age of 412 ka yields a minimum slip-rate of 0.92 ± 0.05 mm.yr$^{-1}$. Assuming that the regional level T3 is coeval at both sites and that the oldest possible age of the youngest sample collected on T3 (i.e., 271 ka) may approximate its abandonment, the slip-rate would be at least 1.40 ± 0.08 mm.yr$^{-1}$. The 25m-deflection of the Marvast River might also be used to estimate the slip-rate on a shorter period of time, but this deflection probably overestimates the true tectonic offset because T1 tread is no longer observed downstream. The offset of the gullies incising both T3 and T2 treads at site Dehshir North is a true tectonic offset. This 20-30m offset provides reliable estimates of the upper and lower bounds of the slip-rate. The offset cannot be older than the OSL age collected below the tread of T2 (OSL1 26.9 ± 1.3 ka) and accounts for a minimum slip-rate greater than 0.71 mm.yr$^{-1}$ (20 m in the last 28.2 ka). The offset cannot be younger than the infilling of T1b and allows determining the upper and lower bounds of the maximum slip-rate. The infilling of T1b being younger than 21.9 ± 1.5 ka, the lower and upper bounds of the maximum slip-rate are respectively 0.85 mm.yr$^{-1}$ (20 m in the last 23.4 ka) and 1.47 mm.yr$^{-1}$ (30 m in the last 20.4 ka). The 12 ± 2m-

651 offset of the riser T1a/T0 at Dehshir North is also an estimate of the actual tectonic offset
652 postdating the emplacement of T1a, which is at most 10.6 ka according to sample OSL IV
653 (Table 3, Figure 13). The 12 ± 2m-offset yields a lower bound of the minimum slip-rate of
654 1.13 ± 0.2 mm.yr$^{-1}$. The early estimate of Nazari et al. (2009) can therefore be refined and the
655 actual slip rate ranges between 0.93 mm.yr$^{-1}$, largest of the conservative estimates of the
656 minimum slip rate, and 1.47 mm.yr$^{-1}$, safe estimate of the maximum slip rate. Therefore, the
657 slip-rate of the Dehshir fault is well determined at 1.2 ± 0.3 mm.yr$^{-1}$ (Figure 15).

658 This study demonstrates the usefulness of combining CRE and OSL data to unravel
659 the abandonment ages of alluvial fans and inset terraces in the desert environment of Central
660 Iran. On the one hand, the use of $^{10}$Be and $^{36}$Cl cosmogenic isotopes with different half-lives
661 allows constraining a very low denudation-rate of 0.001 mm.yr$^{-1}$ for the terrace treads and
662 alluvial fan surfaces of Central Iran. On the other hand, the combination of surface and near-
663 surface sampling exemplifies the occurrence and the variability of inheritance in the
664 cosmogenic isotope concentrations and emphasizes the difficulty in assessing abandonment
665 ages of young alluvial surfaces with CRE measurements in such arid environment (e.g., Le
666 Dortz et al., 2009). The scattering of the CRE surface and near-surface concentrations
667 indicates that the cobbles have not been uniformly exposed to cosmic rays prior to their
668 emplacement. This variable inheritance may originate from a differential exhumation and
669 weathering of the bedrock catchments, or more likely for Dehshir sites, from reworking of
670 cobbles originating from different levels of upper, hence older, fans. The abandonment age of
671 an alluvial surface is thus better estimated by the CRE age of the youngest surface sample
672 than by the weighted mean CRE age of many samples, as already formulated in Mongolia
673 (Vassalo et al., 2007) and along the southern rim of the Tarim basin (Mériaux et al., 2005).
674 However, the youngest sample on a surface may also incorporate inheritance and still
675 overestimate the abandonment age. The amount of CRE inheritance potentially remaining in
676 the youngest sample of a given surface may be obtained by comparing with the OSL age of
677 the late sediments aggraded before the abandonment of the surface. For alluvial surfaces that
678 are young with respect to the considerable amount of inheritance, up to 70 ka in the desert
679 environment of Central Iran, the upper bound on the abandonment age of an alluvial surface
680 appears best estimated by the OSL dating of the late sediment aggraded. For such young
681 surfaces, the CRE measurements are complementary of OSL dating and can be used to
682 unravel the complex history of weathering and transport in the catchment of desert alluvial

683 fans. Finally, such variable CRE inheritance, typifying arid endorheic regions without incision
684 rates, may require more consideration than hitherto drawn for the Andes and Tibet plateaus.
685
686 **Acknowledgments.**
687 This study would have been impossible without financial assistance from INSU-CNRS
688 (PNTS and 3F programs) and CNES-SPOT Image (ISIS program contracts ISIS0403-622 and
689 ISIS0510-812). Université Pierre et Marie Curie (UPMC) and Geological survey of Iran
690 (GSI) provided complementary funding and logistic assistance. KL received a Ministry of
691 Research and Education scholarship granted by the President of UPMC. The $^{10}$Be
692 measurements were performed at the ASTER AMS national facility (CEREGE, Aix en
693 Provence) that is supported by the INSU/CNRS, the French Ministry of Research and Higher
694 Education, IRD and CEA. The $^{36}$Cl measurements were performed at the LLNL-CAMS. We
695 thank L. Leanni, K. Pou, B. Finkel, F. Chauvet, M. Arnold and G. Aumaître for their help
696 during chemistry and measurements at CEREGE and acknowledge B. Oveisi and M.
697 Nazemzadeh for efficient organization and help during fieldwork. We acknowledge thorough
698 reviews by Richard Walker and Anne-Sophie Mériaux. We are very thankful to Anne-Sophie
699 Mériaux for her acute verification of the cosmogenic calculations.
700
701
702 **References**

703 Anderson, R.S., J.L. Repka and G.S. Dick., 1996. Explicit treatment of inheritance in dating
704 depositional surfaces using in situ $^{10}$Be and $^{26}$Al, *Geology*, **24**, 47–51.

705 Arnold M., Merchel S., Bourles D.L., Braucher R., Benedetti L., Finkel R.C., Aumaître G.,
706 Gottdang A. & Klein M., 2010. The French accelerator mass spectrometry facility
707 ASTER: Improved performance and developments. *Nuclear Instruments and*
708 *Methods in Physics Research* B, **268**: 1954–1959.

709 Bateman, M.D., Boulter, C.H., Carr, A.S., Frederick, C.D., Peter, D. and Wilder, M., 2007.
710 Detecting Post-depositional sediment disturbance in sandy deposits using optical
711 luminescence. *Quaternary Geochronology,* **2(1-4)**, 57-64.

712 Berberian, M., 1981. Active faulting and tectonics of Iran, in Zagros, Hindu Kush, Himalaya:
713 geodynamic evolution, *Geodyn. Ser.,* **3,** eds Gupta, H.K. & Delany, F.M., 33–69.

714 Boulter, C., Bateman, M.D. and Frederick, C.D., 2007. Developing a protocol for selecting
715 and dating sandy sites in East Central Texas: Preliminary results. *Quaternary*
716 *Geochronology* **2**, 45-50.

717 Braucher R., Brown E.T., Bourle's D.L., Colin F., 2003. In situ produced $^{10}$Be measurements
718 at great depths: implications for production rates by fast muons. *Earth Planet., Sci.*
719 *Lett.*, **211**, 251-258.
720 Braucher, R., P. Del Castillo, L. Siame , A.J. Hidy , D.L. Bourlès., 2009. Determination of
721 both exposure time and denudation rate from an in situ-produced $^{10}$Be depth profile :
722 A mathematical proof of uniqueness. Model sensitivity and applications to natural
723 cases. *Quaternary Geochronology* **Volume 4,** Issue 1, Pages 1-82
724 Brown, E. T., J. M. Edmond, G. M. Raisbeck, F. Yiou, M. D. Kurz, and E. J. Brook, 1991.
725 Examination of surface exposure ages of Antarctic moraines using in situ produced
726 $^{10}$Be and $^{26}$Al, *Geochim. Cosmochim. Acta*, **55**, 2699 – 2703.
727 Brown, E.T., Bourlès, D.L., Raisbeck, G.M., Yiou, F., Burchfiel, B.C., Molnar, P., Deng, Q.,
728 Li, J., 1998. Estimation of slip rates in the southern Tien Shan using cosmic ray
729 exposure dates of abandoned alluvial fans. *Geol. Soc. Am. Bull.* **110** (3), 377–386.
730 Chmeleff, J., von Blackenburg, F., Kossert, K., Jackob, D., 2010. Determination of the $^{10}$Be
731 half-life by multicollector ICP-MS and liquid scintillation counting. *Nuclear*
732 *Instruments and Methods in Physics Research* B, **268**, 192–199.
733 DeLong, S.B., Arnold, L.J., 2007. Dating alluvial deposits with optically stimulated
734 luminescence, AMS 14C and cosmogenic techniques, western Transverse Ranges,
735 California, USA. *Quat. Geochron.* **2**, 129–136.
736 Desilets, D., Zreda, M., Almasi, P.F., Elmore, D., 2006. Determination of cosmogenic $^{36}$Cl in
737 rocks by isotope dilution: innovations, validation and error propagation. *Chemical*
738 *Geology* **233**, 185-195.
739 Farber, D., Meriaux, A-S., Finkel, R., 2008. Attenuation length for fast nucleon production of
740 $^{10}$Be derived from near-surface production profiles. *Earth and Planetary Science*
741 *Letters* **274**, 295-300.
742 Fattahi, M., Walker, R., Hollingsworth, J., Bahroudi, A., Talebian, M., Armitage, S. and
743 Stokes, S., 2006. Holocene slip-rate on the Sabzevar thrust fault, NE Iran,
744 determined using Optically-stimulated Luminescence (OSL). *Earth and Planetary*
745 *Science Letters*, **245**: 673-684.
746 Fattahi, M., Walker, R., Khatib, M.M., Dolati, A. and Bahroudi, J., 2007. Slip-rate estimates
747 and past earthquakes on the Doruneh fault, eastern Iran. *Geophysical Journal*
748 *International*, **168**: 691-709
749 Fattahi, M., Nazari, H., Bateman, M.D., Meyer, B., Sébrier, M., Talebian, M., Le Dortz, K.,

750 Foroutan, M., Ahmadi Givi, F. and Ghorashi, M., 2010. Refining the OSL age of the
751 last earthquake on the Dheshir fault, Central Iran. *Quat. Geochronology*. **5**, 286–292,
752 Doi:10.1016/j.quageo. 2009.04.005.
753 Galbraith, R. F., Roberts, R.G., Laslett, G.M., Yoshida H., Olley, J.M., 1999. Optical dating
754 of single and multiple grains of quartz from Jinmium rock shelter, northern Australia,
755 part 1, Experimental design and statistical models. *Archaeometry* **41**, 339-364.
756 Gosse, J.C., Phillips, F.M, 2001. Terrestrial in situ cosmogenic nuclides: theory and
757 application. *Quaternary Science Reviews* **20**, 1475-1560.
758 Geological Survey of Iran, 1981. Geological Map of Iran, Ministry of Industry and Mines,
759 scale 1:250 000, Anar quadrangle map.
760 Hetzel, R., Tao, M., Stokes, S., Niedermann, S., Ivy-Ochs, S., Gao, B., Strecker, M.R., Kubik,
761 P.W., 2004. Late Pleistocene/Holocene slip rate of the Zhangye thrust (Qilian Shan,
762 China) and implications for the active growth of the northeastern Tibetan Plateau.
763 *Tectonics* **23** (6), TC6006, doi:10.1029/2004TC001653.
764 Korschinek, G., Bergmaier, A., Faestermann, T., Gerstmann, U. C., Knie, K., Rugel, G.,
765 Wallner, A., Dillmann, I., Dollinger, G., Lierse von Gosstomski, Ch., Kossert, K.,
766 Maiti, M., Poutivtsev, M., Remmert, A., 2010. A new value for the $^{10}$Be half-life by
767 Heavy-Ion Elastic Recoil detection and liquid scintillation counting. *Nuclear*
768 *Instruments and Methods in Physics Research* B, **268**, 187–191.
769 Le Dortz, K., Meyer, B., Sebrier, M., Nazari, H., Braucher, R., Fattahi, M., Benedetti, L.,
770 Foroutan, M., Siame, L., Bourles, D., Talebian, M., Bateman, M.D. and Ghorashi,
771 M., 2009. Holocene right-slip rate determined by cosmogenic and OSL dating on the
772 Anar fault, Central Iran. *Geophys. J. Int.,* **179,** 700–710 Doi:10.1111/j.1365-
773 246X.2009.04309.x.
774 Matmon, O., Simhai, R. Amit, I. Haviv, Y. Enzel, N. Porat, E.V. McDonald, L. Benedetti and
775 R.C. Finkel, 2009. Desert pavement-coated surfaces in extreme deserts present the
776 longest-lived landforms on Earth, *Geol. Soc. Am. Bull.* **121**, pp. 688–697.
777 Merchel S. & Herpers U., 1999. An update on radiochemical separation techniques for the
778 determination of long-lived radionuclides via accelerator mass spectrometry.
779 *Radiochimica Acta,* **84**: 215-219.
780 Merchel S., Arnold M., Aumaître G., Benedetti L., Bourles D.L., Braucher R., Alfimov V.,
781 S.P.H.T. Freeman, Steier P. & Wallner A., 2008. Towards more precise $^{10}$Be and $^{36}$Cl

782 data from measurements at the 10-14 level: Influence of sample preparation. *Nuclear*
783 *Instruments and Methods in Physics Research* B, **266**: 4921-4926.
784 Mériaux, A.-S., Tapponnier, P. Ryerson, F. J. Xiwei, X. King, G. Van der Woerd, J. Finkel,
785 R. C. Haibing, L. Caffee, M. W. Zhiqin, X., 2005. The Aksay segment of the
786 northern Altyn Tagh fault: Tectonic geomorphology, landscape evolution, and
787 Holocene slip rate, *J. Geophys. Res.*, **110**, B04404
788 Meyer, B., Mouthereau, F., Lacombe, O. & Agard, P., 2006. Evidence of quaternary activity
789 along the Deshir Fault, *Geophy. J. int.*, **164**, 192-201.
790 Meyer, B. and K. Le Dortz, 2007. Strike-slip kinematics in Central and Eastern Iran : estimating fault slip-rates averaged over the Holocene. *Tectonics*, **6**, TC5009, doi:10.1029/2006TC002073, 2007.
793 Murray, A.S. and A.G. Wintle, 2000. Luminescence dating of quartz using an improved
794 single-aliquot regenerative-dose protocol, *Radiation Measurements*, **32**, 57-73.
795 Nazari, H., M. Fattahi, B. Meyer, M. Sébrier, M. Talebian, M. Foroutan, K. Le Dortz, M. D.
796 Bateman and M. Ghorashi, 2009. First evidence for large earthquakes on the Deshir
797 fault, Central Iran Plateau. *Terra Nova*, **21**, 417–426.
798 Nissen, E., Walker R.T., Bayasgalan B., Carter A, Fattahi M., Molor E., Schnabel C., West A.
799 J., Xu S., 2009. The late Quaternary slip-rate of the Har-Us-Nuur fault (Mongolian
800 Altai) from cosmogenic $^{10}$Be and luminescence dating, *Earth Planet. Sci. Lett.*
801 doi:10.1016/j.epsl.2009.06.048
802 Owen, L.A., R.C. Finkel, H. Ma, J.Q. Spencer, E. Derbyshire, P. Banard and M.W. Cafee,,
803 2003. Timing and style of late Quaternary glaciation in northeastern Tibet,
804 *Geological Society of America Bulletin* **115**, pp. 1356–1364
805 Owen, L.A., Finkel, R.C., Haizhou, M., Barnard, P.M., 2006. Late Quaternary landscape
806 evolution in the Kunlun Mountains and Qaidam Basin, Northern Tibet: a framework
807 for examining the links between glaciation, lake level changes and alluvial fan
808 formation. *Quat. Int.* **154**–155, 73–86.
809 Repka, J.L., Anderson, R.S., Finkel, R.C., 1997. Cosmogenic dating of fluvial terraces,
810 Fremont River, Utah. *Earth Planet. Sci. Lett.* **152**, 59–73.
811 Roberts, R.G., R.F. Galbraith, H. Yoshida, G.M. Laslett, J.M. Olley, 2000. Distinguishing
812 dose populations in sediment mixtures: a test of single-grain optical dating
813 procedures using mixtures of laboratory-dosed quartz. *Radiation Measurements* **32** ,
814 459-465
815 Schimmelpfennig, I., Benedetti, L., Finkel, R., Pik, R., Blard, P-H., Bourlès, D., Burnard, P.,

816 Williams, A., 2009. Sources of in-situ $^{36}Cl$ in basaltic rocks. Implications for
817 calibration of production rates. *Quaternary Geochronology*, vol **4**, issue 6, 441-461.
818 Siame, L., O. Bellier, R. Braucher, M. Sebrier, M. Cushing, D. Bourlès, B. Hamelin, E.
819 Baroux, B. de Voogd, G. Raisbeck, F. Yiou, 2004. Local erosion rates versus active
820 tectonics : cosmic ray exposure modelling in Provence (south-east France). *Earth*
821 *Planet. Sci. Lett*, **220**, 3-4, 345-364,
822 Stone, J. O. H., Allan, G. L., Fifield, L. K., Cresswell, R. G., 1996. Cosmogenic chlorine-36
823 from calcium spallation, *Geochim. Cosmochim. Acta*, **60**, 679-692.
824 Stone, J. O., Evans, J. M., Fifield, L. K., Allan, G. L., Cresswell, R. G., 1998. Cosmogenic
825 chlorine-36 production in calcite by muons, *Geochim. Cosmochim. Acta*, **62**, 433-
826 454.
827 Stone J. O., 2000. Air pressure and cosmogenic isotope production. *J. Geophys. Res.*, **105**,
828 B10, 23753-23759.
829 Vassallo R, Ritz J, F., Braucher R, Jolivet M, Carretier S, Larroque C, Chauvet A, C. Sue C,
830 Todbileg M, Bourlès D, Arzhannikova A, Arzhannikov S., 2007. Transpressional
831 tectonics and stream terraces of the Gobi-Altay, Mongolia. *Tectonics* **26**, TC5013,
832 doi:10.1029/2006TC002081.
833 Vermeesch, P., 2007. CosmoCalc: An Excel add-in for cosmogenic nuclide calculations,
834 *Geochem. Geophys. Geosyst.,* **8**, Q08003, doi:10.1029/2006GC001530.
835 Walker, R. and J. Jackson, 2004. Active tectonics and late Cenozoic strain distribution in
836 central and eastern Iran, *Tectonics*, **23**, TC5010, doi:10.1029/2003TC001529.
837 Zreda, M. G., Philips, F. M., Elmore, D., Kubik, P. W., Sharma, P., Dorn, R. I., 1991.
838 Cosmogenic chlorine-36 production rates in terrestrial rocks, *Earth Planet. Sci. Lett.*,
839 **105**, 94-109.
840

840 **Figures captions**

841

842 Figure1: Spot imagery of the southern part of the Dehshir fault, near Marvast town. The fault
843 cuts across abandoned alluvial fan systems and active rivers. Boxes indicate locations of
844 Figures 2 and 4. The inset is a Landsat mosaic of the Dehshir fault and surroundings. The
845 Nain Baft ophiolite outcrops are stylized in purple. The total dextral offset of the fault (65 ±
846 15 km) is outlined by the displacement of the suture.

847

848 Figure 2: Site Dehshir South. a) Quickbird imagery. The fault trace cuts across the Marvast
849 River, intermittent channels and successive abandoned fans and terraces (T3 in orange, T2 in
850 yellow, T1 a and b in green). The numbered dots show the position of the surface samples
851 collected for $^{10}$Be and $^{36}$Cl CRE dating (red and blue dots, respectively). The black squares
852 show the position of the near-surface samples collected along depth profiles PS1 and PS2
853 (Figure 11, 12 and 13). The black dots locate the OSL samples taken below the ground
854 surface. AB locates the topographic profile of figure 3. b) Close up on the 380 ± 20m dextral
855 offset of a river course, incised within the oldest (T3) fan surface.

856

857 Figure 3: a) Topographic profile across the abandoned fan system (see location on figure 2)
858 highlights the relative elevation of the terraces and their degree of incision by the Marvast
859 river. The profile is work out from a differential GPS survey. b) Field photograph of the inset
860 terraces. Location of OSL III and IV are indicated on the close up pictures of the risers
861 T1b/T0 and T1a/T0 respectively.

862

863 Figure 4: Site Dehshir North. a) Quickbird imagery. Different coloured shading denotes the
864 successive abandoned fans (same code as for Figure 2). Numbered dots show the position of
865 the surface samples collected for $^{10}$Be and $^{36}$Cl CRE dating (red and blue dots, respectively).
866 The black square shows the position of the near-surface samples collected along the depth
867 profiles PN (Figure 7 and 8). The black dots locate the OSL samples taken below the ground
868 surface. Rectangle denotes the close up on the offset riser on figure 5. Dotted circles indicate
869 location of 20-30 m right-lateral offset-gullies. Black (AB and CD) and white (RI) lines locate
870 topographic sections on each side of the fault and on the riverbed respectively. b)
871 Topographic profiles, achieved from differential GPS survey and projected along fault strike,
872 highlight the amount of stream incision upstream and down stream of the fault. The offset-
873 gullies are indicated.

874

875 Figure 5: a) Raw (left panel) and interpreted (right panel) images of the dextral offset of the
876 recent riser (T1a/T0). Open triangles point to the fault trace and arrows to the foot of the riser.
877 Rectangle denotes the enlargement on the offset-riser b) Quickbird image wrapped on the
878 digital elevation model worked out from a DGPS survey. c) Enlargement on the 12 ± 2 m
879 offset-riser (T1a/T0 downstream, T3/T0 upstream). The blue line denotes the base of the riser.
880 d) Field photograph of the offset-riser with vertical arrows pointing to the foot of the riser.

881

882 Figure 6: Summary of observations at site Dehshir North. a) $^{10}$Be and $^{36}$Cl CRE ages of
883 surface samples modelled without erosion and without inheritance are indicated by red and
884 blue dots above each surface. The shaded columns extend from the minimum age to the
885 maximum age given by the error bars of the samples. The OSL samples collected beneath
886 each surface are indicated in stratigraphic order (see text for discussion). The plot of CRE
887 ages is given for each surface sample, in relative position from north to south. Dots and errors
888 bars are in red and blue for $^{10}$Be and $^{36}$Cl, respectively. b) Distribution of *in-situ* produced $^{10}$Be
889 (left panel) and $^{36}$Cl (right panel) CRE ages modelled without erosion and without inheritance
890 for the surface samples collected on T3 tread. The thin curves represent the CRE age
891 probability as Gaussian distribution for each individual sample and the thick curves
892 correspond to the summed Gaussian density probability function. The weighted mean CRE
893 age is obtained with errors equal to two standard deviations ($2\sigma$). Outlier sample DN06S2
894 (235.5 ± 35.4 ka) has not been included in the $^{10}$Be statistics.

895

896 Figure 7: Summary of observations at site Dehshir South. a) $^{10}$Be and $^{36}$Cl CRE ages of
897 surface samples modelled without erosion and without inheritance are indicated by red and
898 blue dots above each surface. The shaded columns extend from the minimum age to the
899 maximum age given by the error bars of the samples. The OSL samples collected beneath
900 each surface are indicated in stratigraphic order (see text for discussion). The plot of CRE
901 ages is given for each surface sample, in relative position from north to south. Dots and errors
902 bars are in red and blue for $^{10}$Be and $^{36}$Cl, respectively. b) Distribution of in situ produced $^{10}$Be
903 (left) and $^{36}$Cl (right) CRE ages modelled without erosion and without inheritance for the
904 surface samples collected on T3 Tread. The thin curves represent the CRE age probability as
905 Gaussian distribution for each individual sample and the thick curves correspond to the

906 summed Gaussian density probability function. The weighted mean age is obtained with
907 errors equal to two standard deviations (2 σ ).
908
909 Figure 8: Plot of the near-surface, measured $^{36}Cl$ concentrations (black dots) as a function of
910 depth at profile PN (location on figure 4). Surface samples (blue dots) are shown but not
911 included in the modelling. The erosion rate is modelled for a 3 Ma-old surface to ensure that
912 the steady state equilibrium between production and disintegration has been reached. For the
913 three different densities tested (obtained from the near-surface samples), the best-fit erosion
914 rate – inheritance is indicated.
915
916 Figure 9. a) Plot of the near-surface, measured $^{10}Be$ concentrations (black dots) as a function
917 of depth at profile PN (location on figure 4). Surface samples are indicated as red dots. The
918 modelled curves fit distributions of concentrations, without erosion, and for three assigned
919 inheritances. The modelling includes both the near-surface samples and the weighted mean
920 age of the surface samples (DN06S2 excluded). b) Log ($\chi^2$) values for a range of inheritance
921 and CRE ages modelled without erosion are plotted below. T he modelling converges towards
922 a best-fit age of 460 ka and inheritance 3.8 $10^5$ at.$g^{-1}$($SiO_2$) (star).
923
924 Figure 10: Weighted mean $^{10}Be$ CRE age of T3 tread including the surface sample exposure
925 ages of North and South sites and excluding outlier sample DN06S2. The thin curves
926 represent the CRE age probability as Gaussian distribution for each individual sample and the
927 thick curves correspond to the summed Gaussian density probability function. The weighted
928 mean age is obtained with errors equal to two standard deviations (2 σ ).
929
930 Figure 11: a) Weighted mean CRE age for the $^{10}Be$ and $^{36}Cl$ surface samples collected on T2
931 tread at Dehshir South site. The ages have been calculated assuming no erosion and no
932 inheritance and the sample DS08S114 (49.9 ± 3.3 ka) has not been included in the statistics.
933 The thin curves represent the CRE age probability as Gaussian distribution for each individual
934 sample and the thick curves correspond to the summed Gaussian density probability function.
935 The weighted mean age is obtained with errors equal to two standard deviations (2 σ ). b)
936 Field photograph showing the 4m high T2/T0 riser sampled for profile PS1 (see Figure 2 for
937 location). c) Profile of $^{10}Be$ concentrations through the terrace T2 at site PS1. Red and blue
938 dots are surface and near-surface samples, respectively. The two OSL samples collected by

939 the same riser along strike within sandy lenses are indicated. Dashed curves represent the
940 forward models of theoretical $^{10}$Be near-surface concentration for a 30 ka abandonment age
941 assuming homogeneous inheritances of 3.5 $10^5$ at.g$^{-1}$($SiO_2$) (left) and 9 $10^5$ at.g$^{-1}$($SiO_2$) (right).
942
943 Figure 12: Plot of the measured $^{10}$Be concentrations as a function of depth (left panel) and
944 simplified stratigraphy (right panel) through profile PS2. Depth profile PS2 has been
945 excavated within T2 tread, North of the Marvast River (see location on figure 2). Relative
946 positions of OSL samples AB/2006/I and II and CRE near-surface amalgams are shown
947 (blacks arrows).
948
949 Figure 13: Synthesis of observations and plot of sample ages in relative position from north to
950 south for site Dehshir North (left panels) and site Dehshir South (right panels). Dots and
951 errors bars are in red, blue and black for $^{10}$Be, $^{36}$Cl and OSL dating, respectively. a) The thick
952 lines and shaded regions are the weighted mean with 2σ confidence interval for the CRE
953 surface age. Samples DN06S2 and DN08S114 have been omitted for the T3 and T2 statistics,
954 respectively. The thin lines are the oldest possible CRE age of the youngest CRE sample
955 collected on the terrace treads. b) Upper part, relative positions and OSL ages of the samples
956 collected below the terrace treads of T2, T1b and T1a. Samples HI (Nazari et al., 2009;
957 Fattahi et al., 2010) and AB have been collected within trenches excavated for paleoseismic
958 purposes and samples OSL I-IV by the terrace risers. Lower part, CRE and OSL ages
959 available for terraces T2 and T1. The thick black line is the oldest possible age of the most
960 surficial OSL sample collected below each terrace tread.
961
962 Figure 14: Depth-profile PS1 and PN of $^{10}$Be concentrations respectively through terrace T2
963 (a) and T3 (b). Violet and red dots are the measured concentrations of the near-surface
964 amalgams and surface samples, respectively. Blue dots and black dots are the respective
965 concentrations of the near-surface amalgams and surface samples once one near-surface
966 amalgam is restored to a null concentration without bringing back any other near-surface
967 sample to a negative concentration (see text for discussion). The time of *in-situ* exposure to
968 bring that near-surface sample to its measured concentration is indicated in red, and the
969 residual concentrations remaining in the other near-surface samples by black arrows
970 materializing the sample inheritance for such duration of exposure. The only rejuvenated
971 surface sample displaying a negative concentration is the sample DN06S2 on T3, therefore a

statistical and physical outlier for a 412 ka exposure age. This race to zero-concentration for the near-surface amalgams indicates that T2 and T3 have to be younger than 107 ka and 412 ka, respectively. Shaded area corresponds to physically unrealistic domains of negative $^{10}$Be concentrations.

Figure 15: Summary of offsets and ages available to assess the slip-rate of the Dehshir fault. Dashed boxes and boxes correspond to weighted mean CRE age with and without removal of the estimated inheritance (see text for discussion). The oldest possible abandonment ages of T3 and T2 (thick vertical black lines) are determined from the near-surface concentrations (Figure 14). The exposure age of the youngest sample (black cross) on each terrace is also indicated. Grey boxes correspond to the OSL age domains of the late sediments emplaced below the treads of T2 and T1. Light grey slip-rate domain is the range of minimum slip-rate of Nazari et al. (2009). The dark grey domain narrows the uncertainties and demonstrates the Dehshir fault slips faster than 0.93 mm.yr$^{-1}$ but slower than 1.47 mm.yr$^{-1}$.

Table 1: The $^{10}$Be and $^{36}$Cl nuclide concentrations and CRE modelled ages for surface and near-surface samples along the Dehshir fault. Propagated analytical uncertainties include error blank, carrier and counting statistics. Zero erosion model ages are calculated for surface samples with propagated analytical uncertainties, including error blank, carrier and counting statistic; corresponding geographic correction factors and without shielding in agreement with site topography. $^{10}$Be and $^{36}$Cl half-life are respectively 1.387 Ma (Chmeleff et al., 2010; Korshincek et al., 2010) and 301 ka (Gosse & Philipps, 2001). For surface samples, a density of 2.2 g.cm$^{-3}$ and 2 g.cm$^{-3}$ have been used for quartz and carbonates samples respectively. An attenuation length of 160 g.cm$^{-2}$ (Gosse & Philipps, 2001) has been used. Stone (2000) polynomial has been used to determine surficial production rate assuming a SLHL production rate of 4.49 at.g$^{-1}$.yr$^{-1}$ for $^{10}$Be with 6% of uncertainty. The $^{36}$Cl production rate of 48.8 ± 3.4 at.g$^{-1}$.yr$^{-1}$ is from Stone (1996). $^{10}$Be ages have been calculated using Cosmocalc (Vermeesh 2007). $^{36}$Cl ages have been calculated using Excel spreadsheet of Schimmelpfening et al. (2009). N.M means no or incoherent measure. Maximum erosion rates have been calculated for the surface cobbles collected on T3 tread, with an infinite time of exposure hence at the steady state equilibrium. About 20-30 pebbles with centimetre size have been generally collected for the amalgamated samples of the profiles. For the T2/T0 riser profile, the amalgams are made of a dozen of larger cobbles.

1005

1006 Table 2: Mean chemical composition of the samples collected for $^{36}Cl$ dating. Measurements
1007 of the major elements were undertaken at the SARM facility (Nancy, France).

1008

1009 Table 3: Equivalent dose ($D_e$), annual dose rate ($D_a$) and calculated OSL ages for each sample.
1010 The weighted mean ages published in Nazari et al. (2009) have been refined following the
1011 statistical analysis used by Fattahi et al (2010) to account for partial bleaching. Ages have
1012 been calculated for Quartz grains with size ranging between 90 and 150 microns.

1013

1014

1015

Figure 1

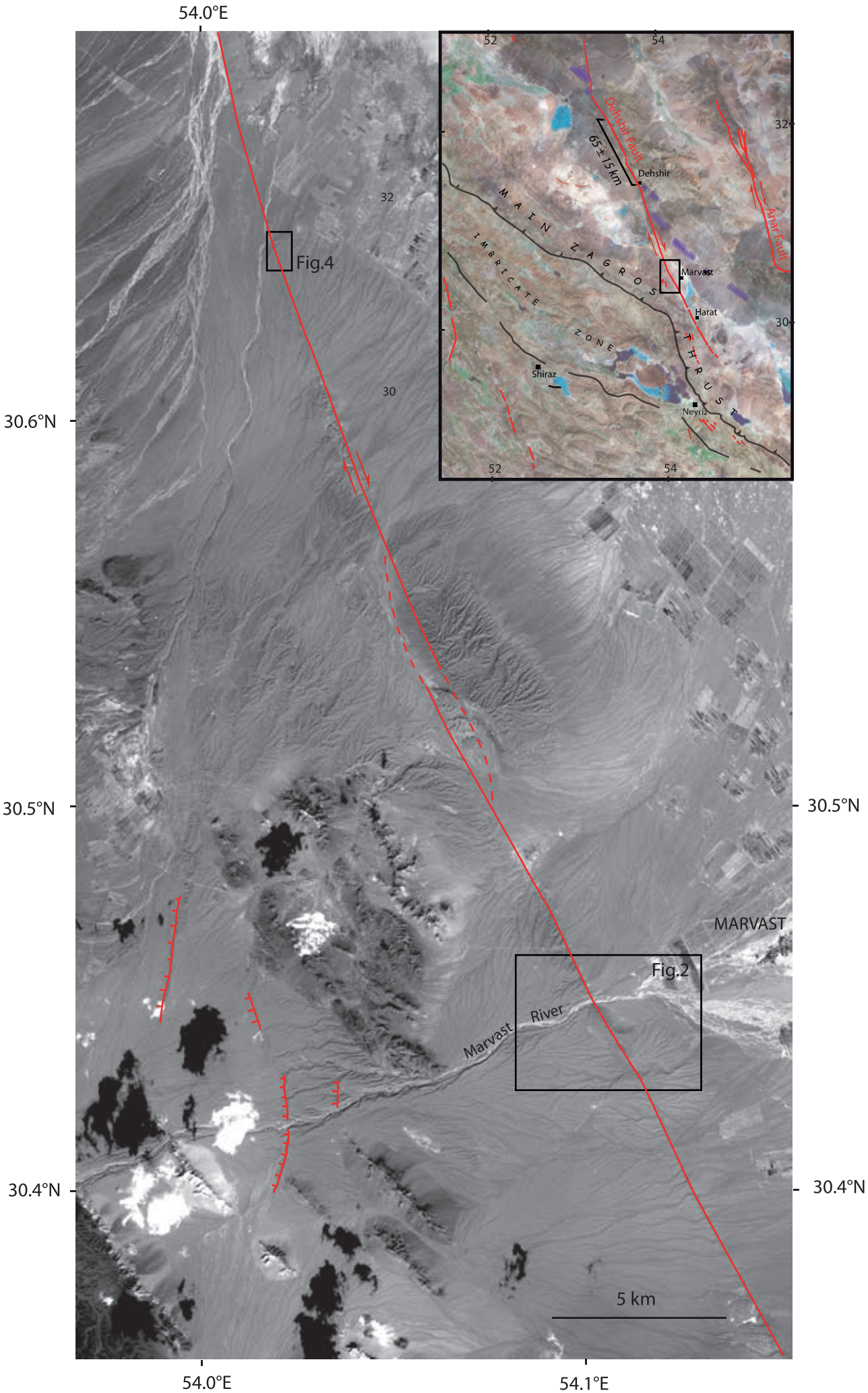
54.0°E
30.6°N
30.5°N
30.4°N
54.0°E
54.1°E
30.5°N
30.4°N
32
30
Fig.4
Fig.2
MARVAST
Marvast River
5 km
52
54
32
30
Dehshir Fault
65±15km
Dehshir
Anar Fault
MAIN ZAGROS
IMBRICATE ZONE
THRUST
Marvast
Harat
Shiraz
Neyriz

Figure 2

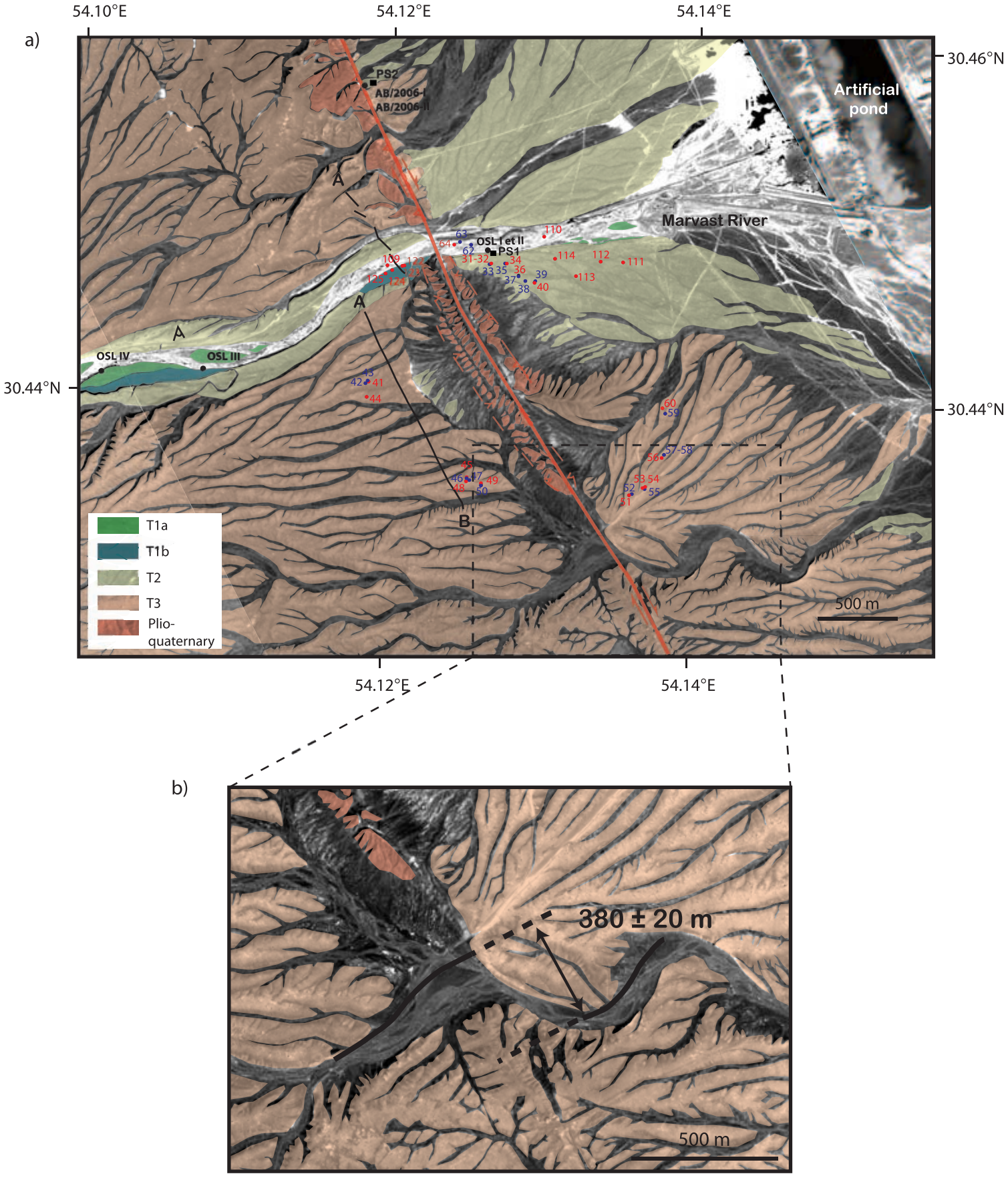
a)
54.10°E
54.12°E
54.14°E
30.46°N
30.44°N
PS2
AB/2006-I
AB/2006-II
Artificial pond
Marvast River
OSL I et II
PS1
OSL IV
OSL III
A
B
T1a
T1b
T2
T3
Plio-quaternary
500 m
b)
380 ± 20 m
500 m

Figure 3

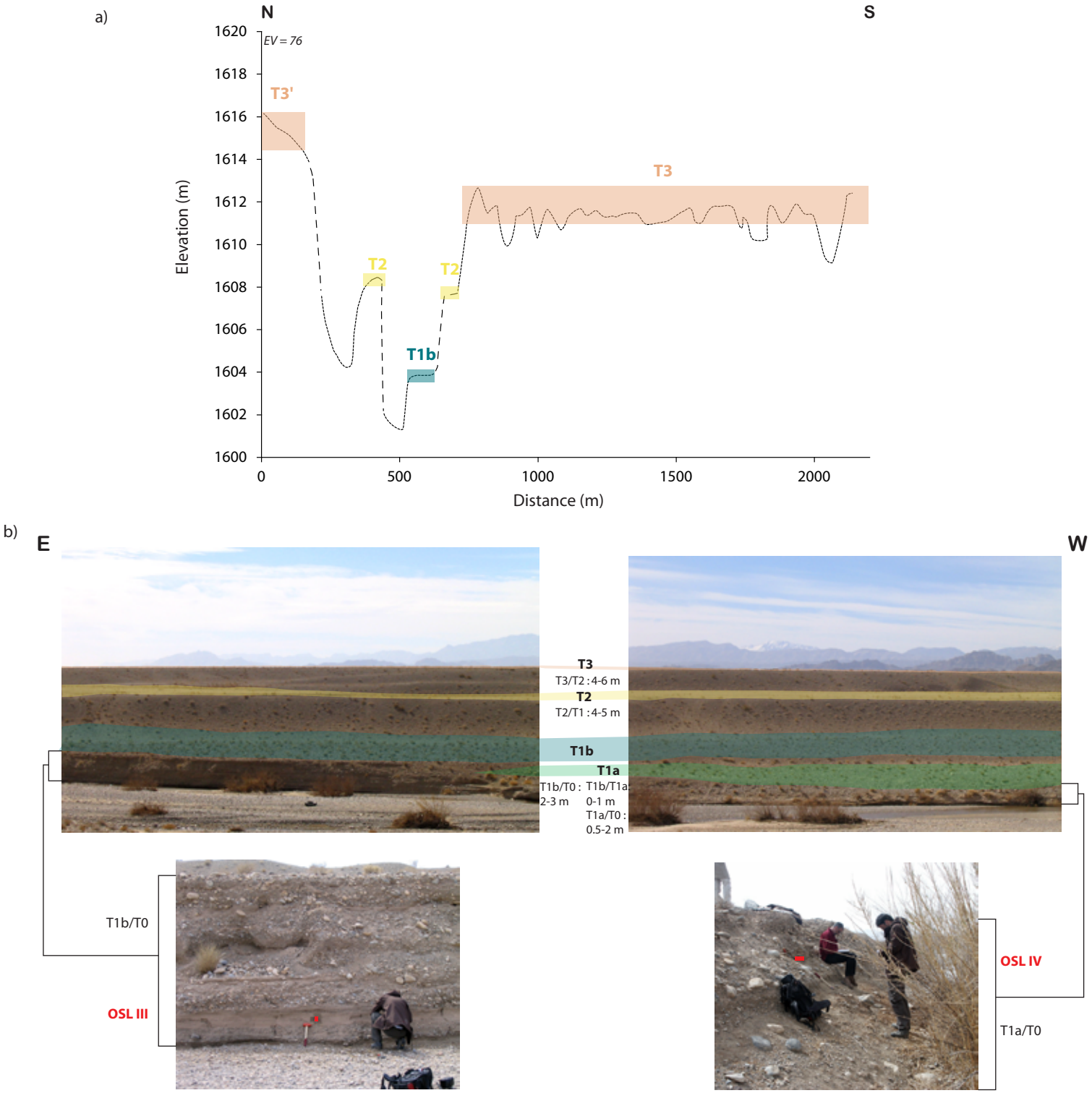
a)
N
S
EV = 76
T3'
T3
T2
T2
T1b
Elevation (m)
1620
1618
1616
1614
1612
1610
1608
1606
1604
1602
1600
0
500
1000
1500
2000
Distance (m)
b)
E
W
T3
T3/T2 : 4-6 m
T2
T2/T1 : 4-5 m
T1b
T1a
T1b/T0 : 2-3 m
T1b/T1a 0-1 m
T1a/T0 : 0.5-2 m
T1b/T0
OSL III
OSL IV
T1a/T0

Figure 4

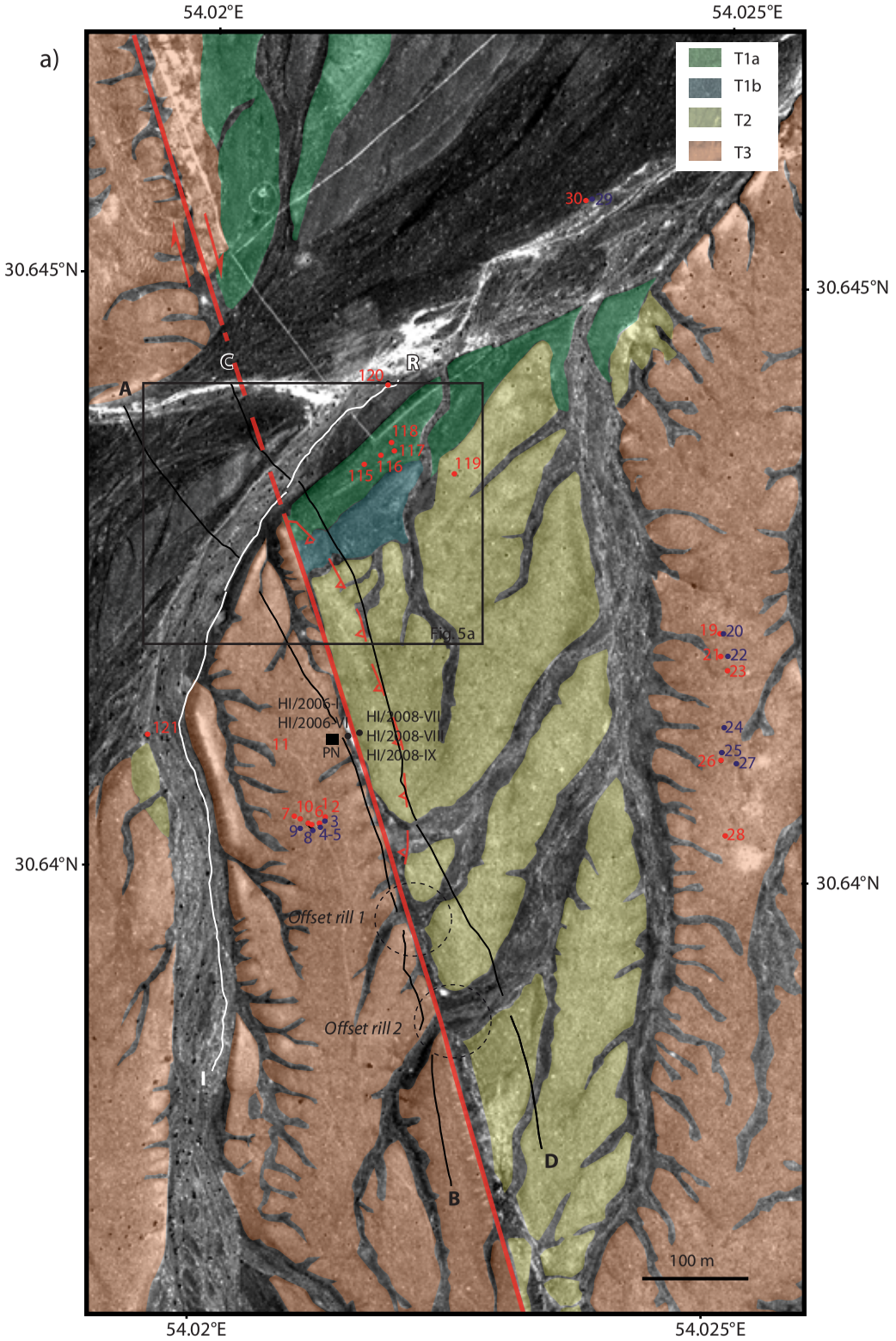
a)
54.02°E
54.025°E
30.645°N
30.64°N
T1a
T1b
T2
T3
A
B
C
D
R
Fig. 5a
Offset rill 1
Offset rill 2
HI/2006-I
HI/2006-VI
HI/2008-VII
HI/2008-VIII
HI/2008-IX
PN
100 m

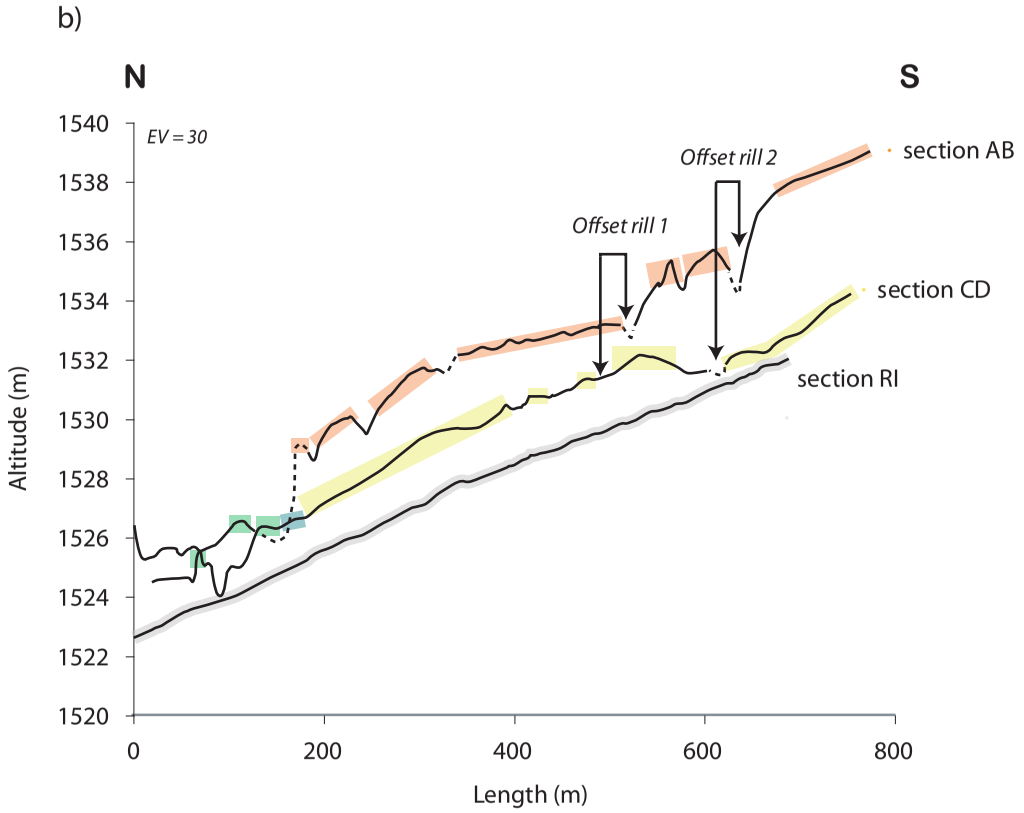
b)
N
S
EV = 30
Altitude (m)
Length (m)
Offset rill 1
Offset rill 2
section AB
section CD
section RI

Figure 5

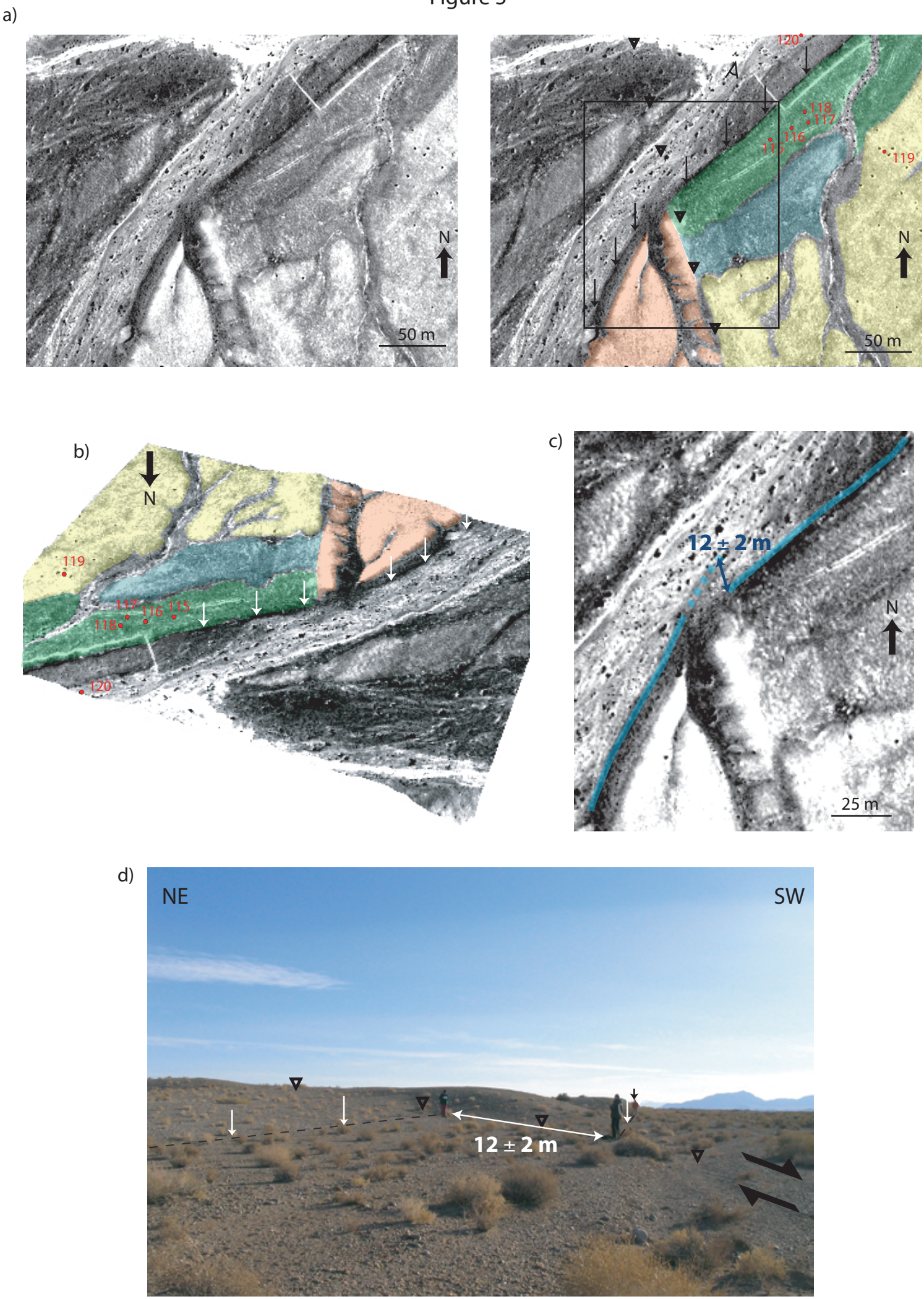
a)
N
50 m
A
120
118
117
116
115
119
N
50 m
b)
N
119
117
116
115
118
120
c)
12 ± 2 m
N
25 m
d)
NE
SW
12 ± 2 m

Figure 6

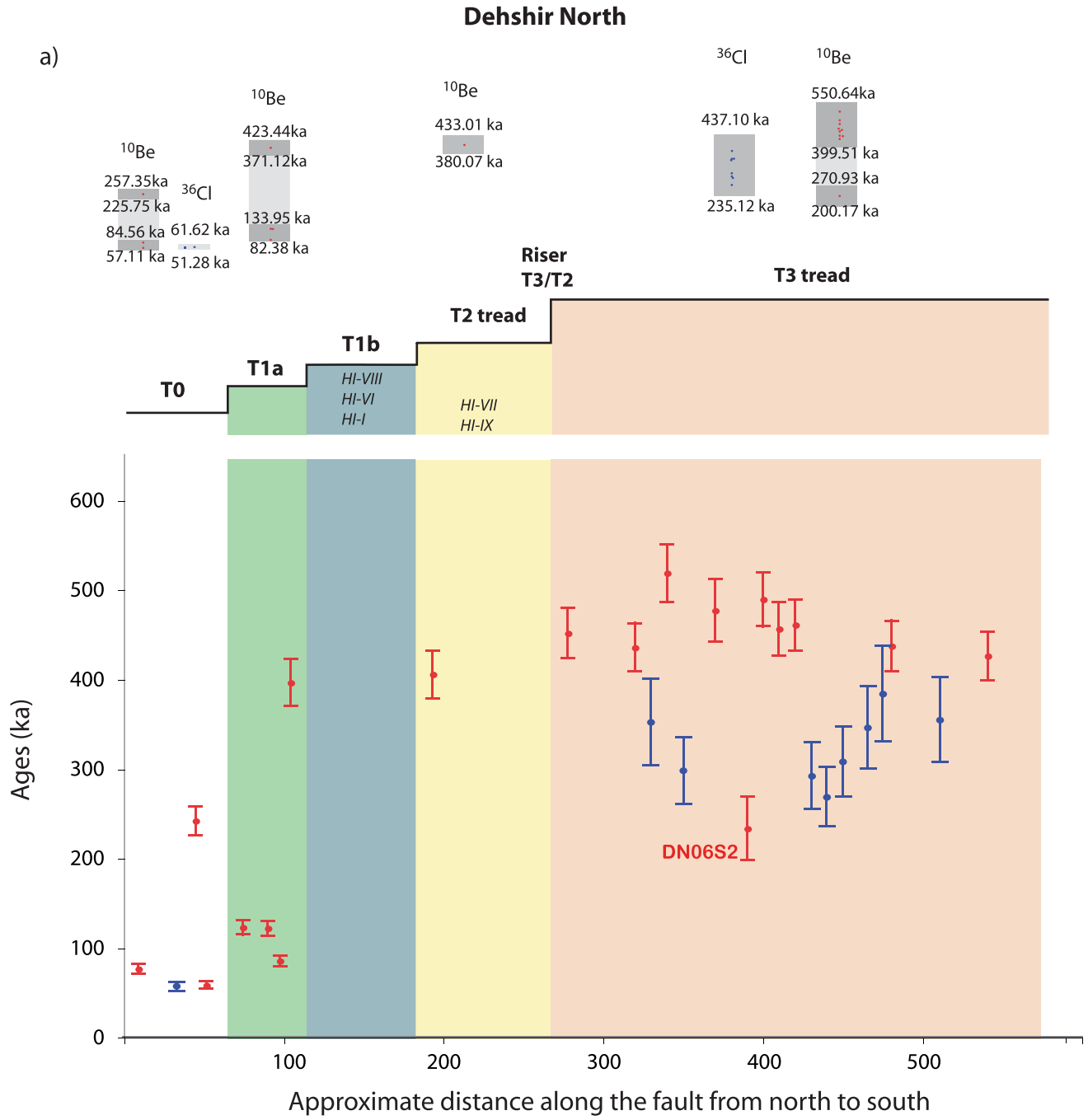
Dehshir North
a)
10Be
257.35ka
225.75 ka
84.56 ka
57.11 ka
36Cl
61.62 ka
51.28 ka
10Be
423.44ka
371.12ka
133.95 ka
82.38 ka
10Be
433.01 ka
380.07 ka
36Cl
437.10 ka
235.12 ka
10Be
550.64ka
399.51 ka
270.93 ka
200.17 ka
Riser
T3/T2
T3 tread
T2 tread
T1b
T1a
T0
HI-VIII
HI-VI
HI-I
HI-VII
HI-IX
DN06S2
Ages (ka)
0
100
200
300
400
500
600
100
200
300
400
500
Approximate distance along the fault from north to south

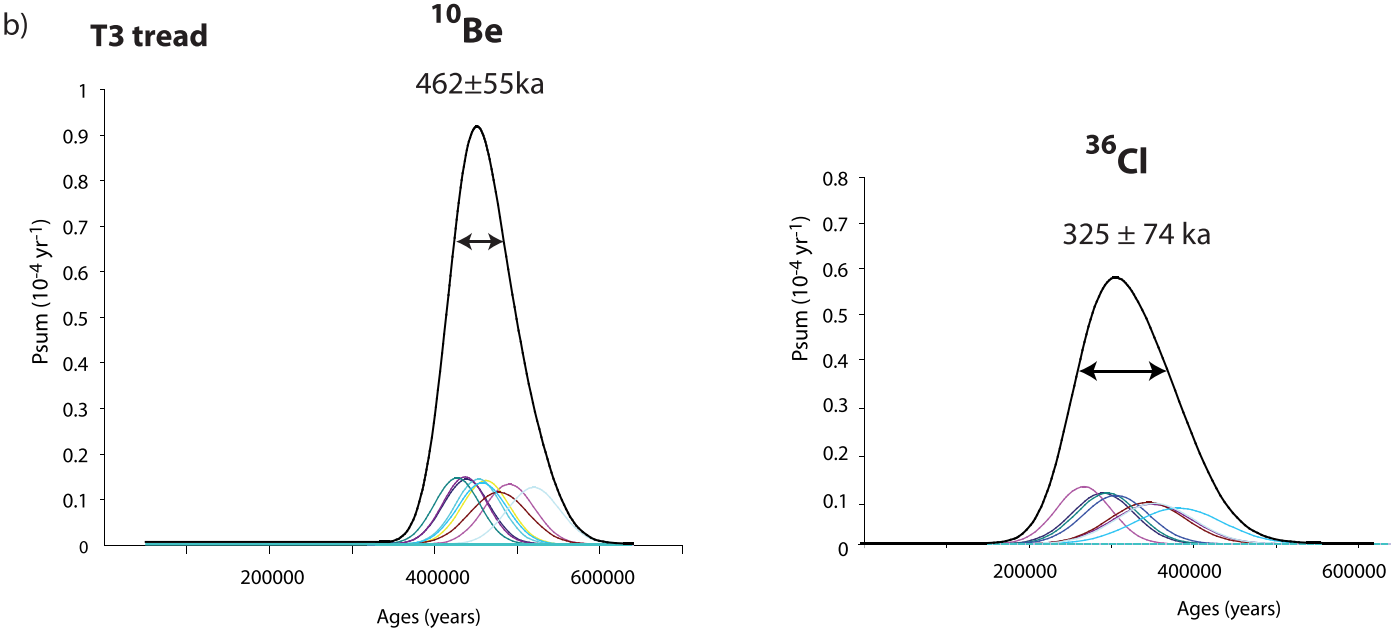
b)
T3 tread
10Be
462±55ka
Psum (10-4 yr-1)
0
0.1
0.2
0.3
0.4
0.5
0.6
0.7
0.8
0.9
1
200000
400000
600000
Ages (years)
36Cl
325 ± 74 ka
Psum (10-4 yr-1)
0
0.1
0.2
0.3
0.4
0.5
0.6
0.7
0.8
200000
400000
600000
Ages (years)

Figure 7

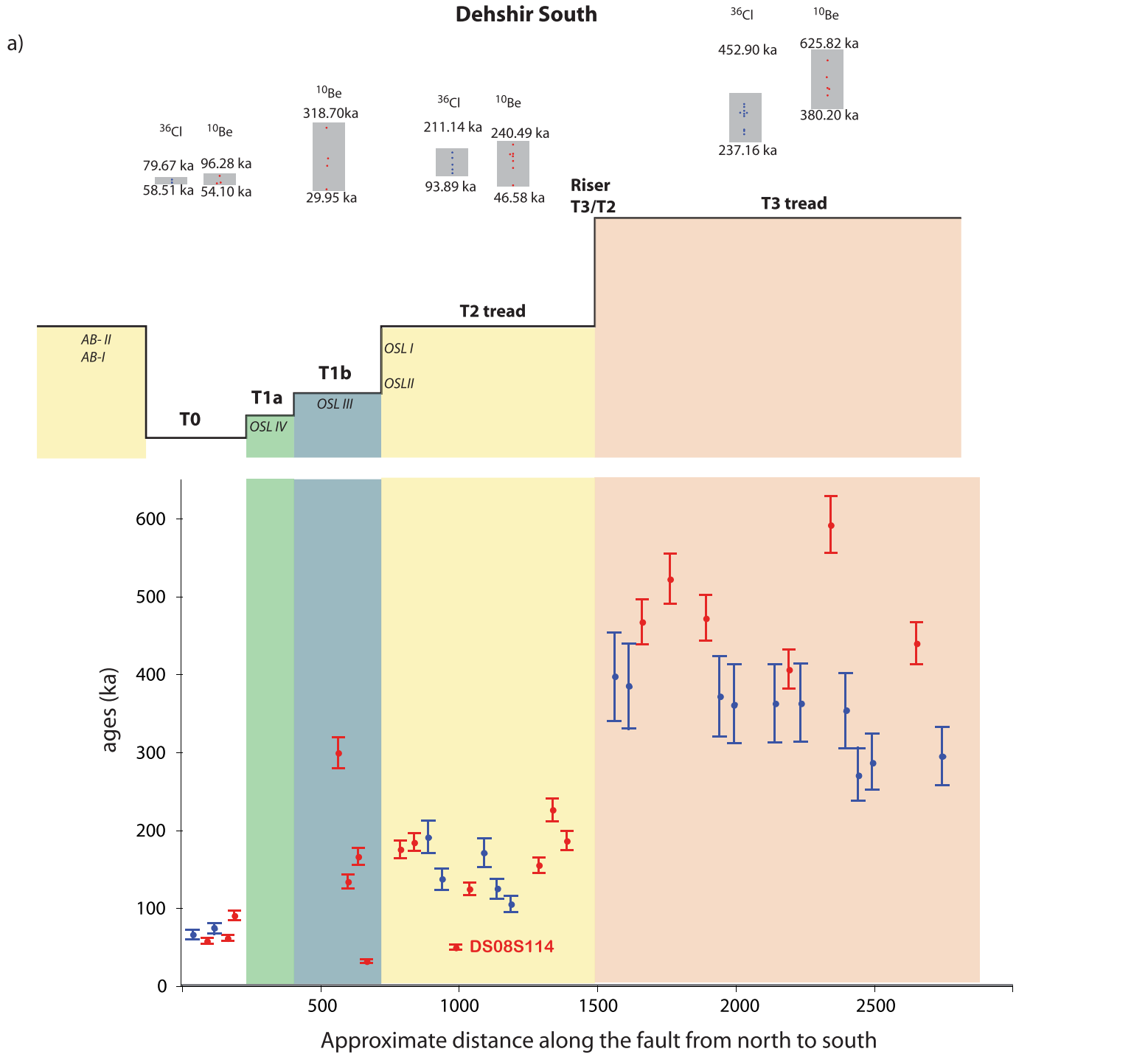
a)
Dehshir South
36Cl
10Be
79.67 ka
96.28 ka
58.51 ka
54.10 ka
10Be
318.70ka
29.95 ka
36Cl
10Be
211.14 ka
240.49 ka
93.89 ka
46.58 ka
36Cl
10Be
452.90 ka
625.82 ka
380.20 ka
237.16 ka
Riser
T3/T2
T3 tread
T2 tread
AB- II
AB-I
T0
T1a
OSL IV
T1b
OSL III
OSL I
OSLII
ages (ka)
600
500
400
300
200
100
0
DS08S114
500
1000
1500
2000
2500
Approximate distance along the fault from north to south

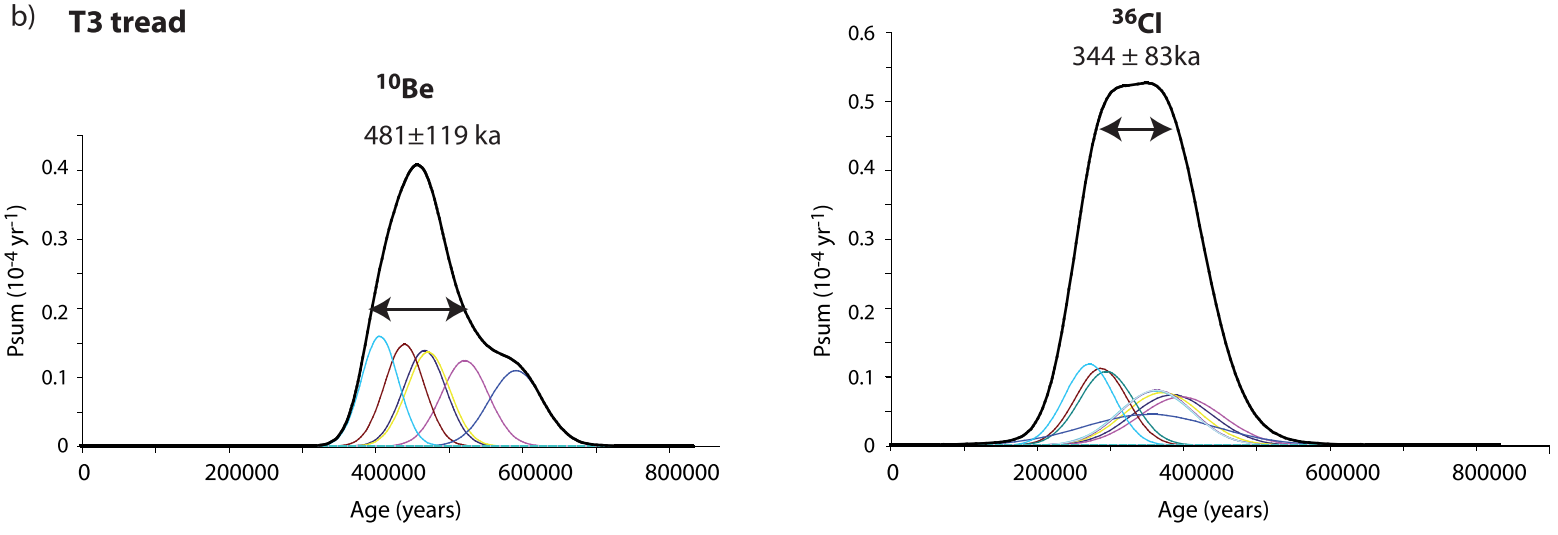
b)
T3 tread
10Be
481±119 ka
Psum (10-4 yr-1)
0.4
0.3
0.2
0.1
0
0
200000
400000
600000
800000
Age (years)
36Cl
344 ± 83ka
0.6
0.5
0.4
0.3
0.2
0.1
0
0
200000
400000
600000
800000
Age (years)

Figure 8

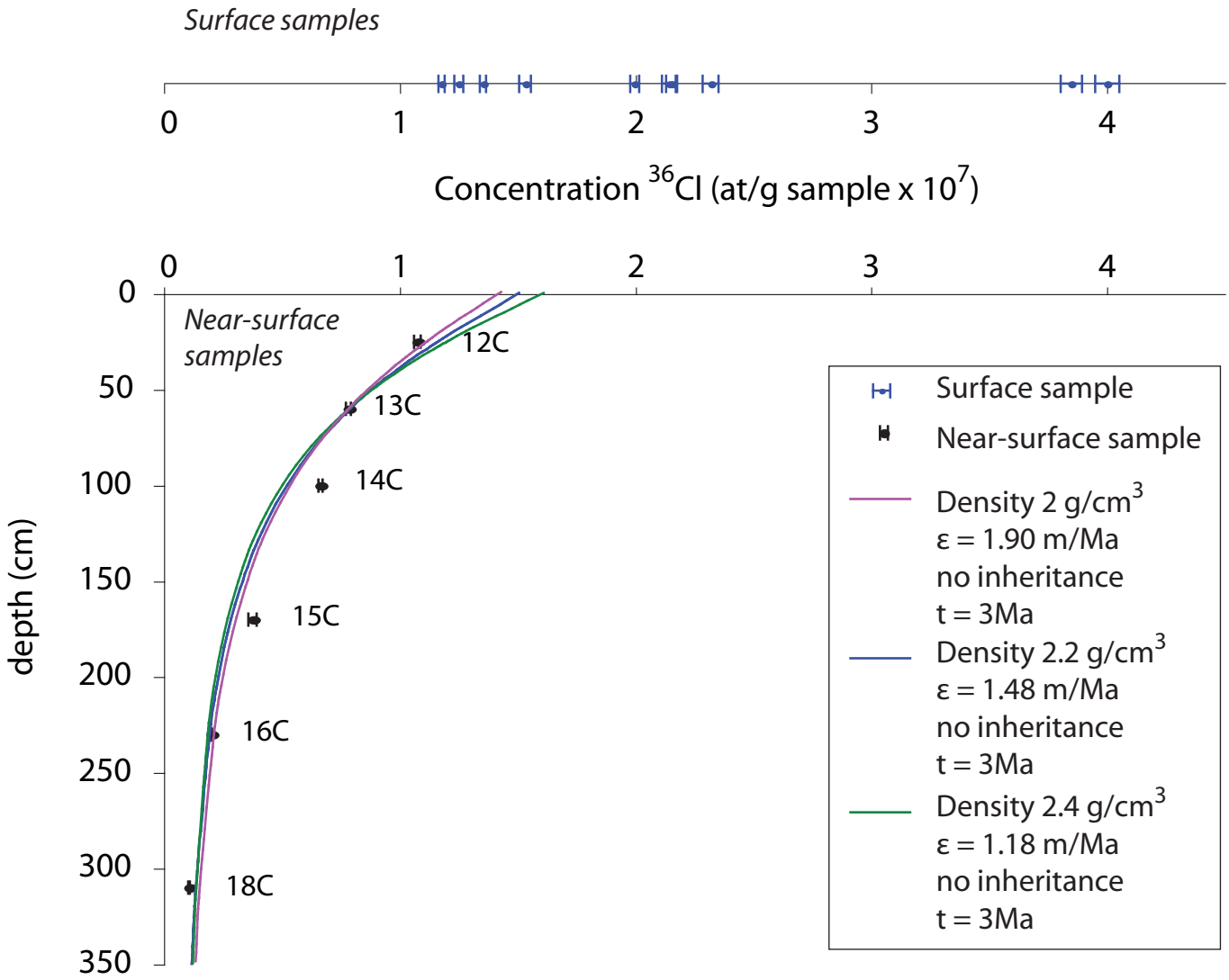
Surface samples
0
1
2
3
4
Concentration $^{36}$Cl (at/g sample x $10^7$)
0
1
2
3
4
0
50
100
150
200
250
300
350
depth (cm)
Near-surface samples
12C
13C
14C
15C
16C
18C
Surface sample
Near-surface sample
Density 2 g/cm$^3$
ε = 1.90 m/Ma
no inheritance
t = 3Ma
Density 2.2 g/cm$^3$
ε = 1.48 m/Ma
no inheritance
t = 3Ma
Density 2.4 g/cm$^3$
ε = 1.18 m/Ma
no inheritance
t = 3Ma

Figure 9

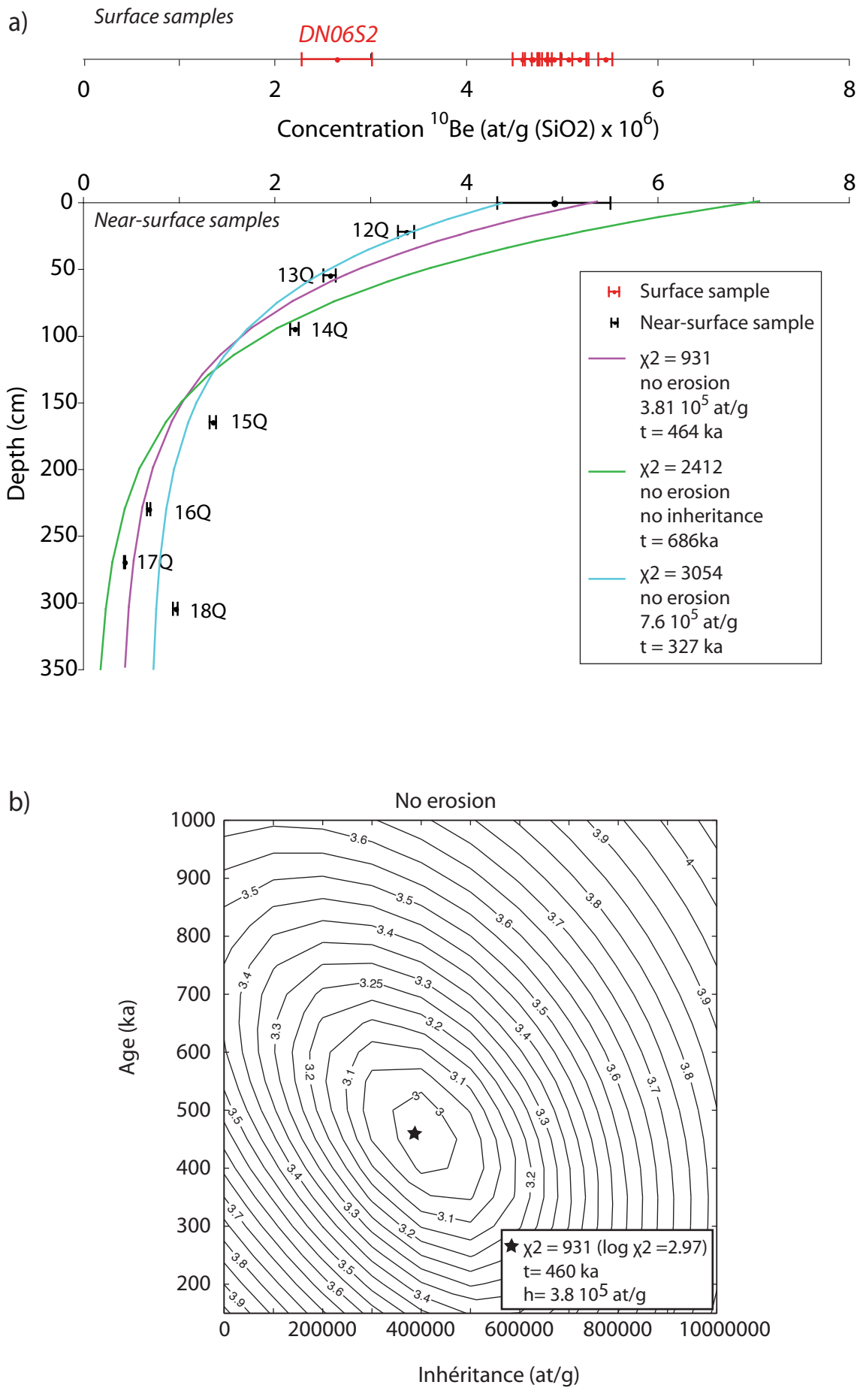
a)
Surface samples
DN06S2
0
2
4
6
8
Concentration $^{10}$Be (at/g (SiO2) x $10^6$)
Near-surface samples
12Q
13Q
14Q
15Q
16Q
17Q
18Q
Depth (cm)
0
50
100
150
200
250
300
350
Surface sample
Near-surface sample
χ2 = 931
no erosion
3.81 $10^5$ at/g
t = 464 ka
χ2 = 2412
no erosion
no inheritance
t = 686ka
χ2 = 3054
no erosion
7.6 $10^5$ at/g
t = 327 ka
b)
No erosion
Age (ka)
1000
900
800
700
600
500
400
300
200
0
200000
400000
600000
800000
10000000
Inhéritance (at/g)
χ2 = 931 (log χ2 =2.97)
t= 460 ka
h= 3.8 $10^5$ at/g

Figure 10

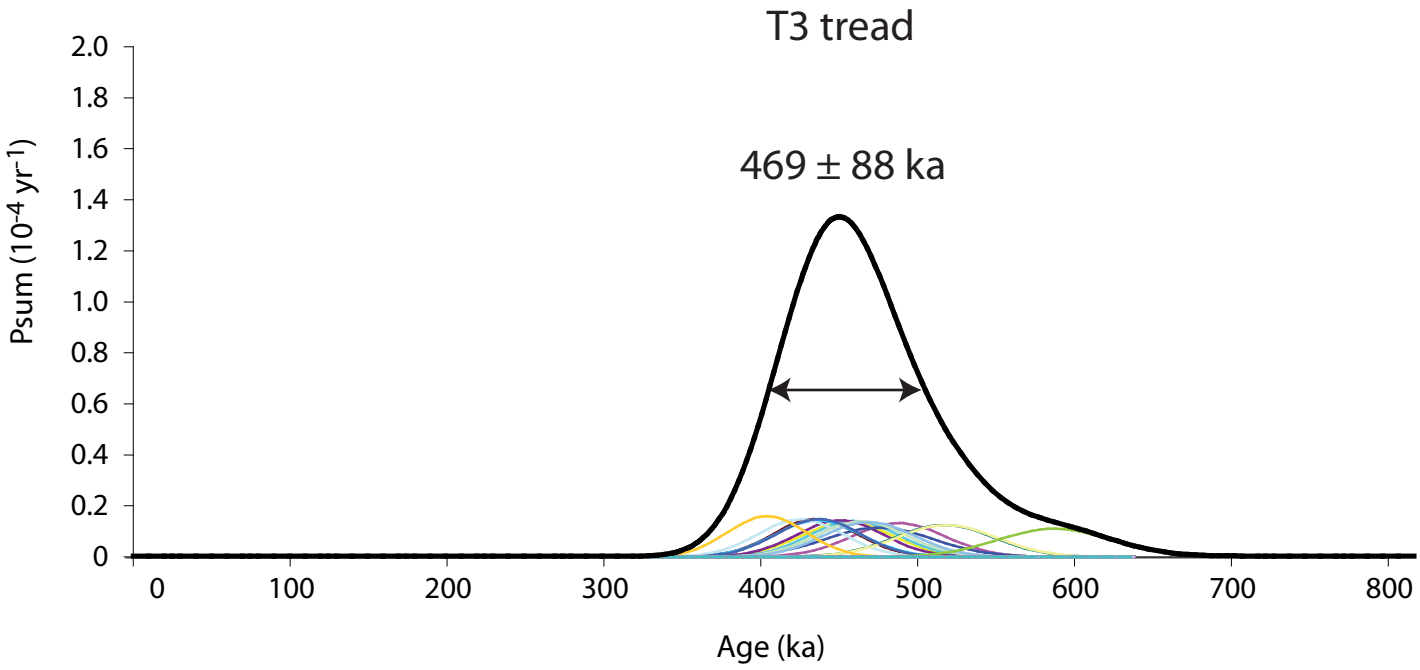
T3 tread
469 ± 88 ka
Psum (10-4 yr-1)
2.0
1.8
1.6
1.4
1.2
1.0
0.8
0.6
0.4
0.2
0
0
100
200
300
400
500
600
700
800
Age (ka)

Figure 11

a)

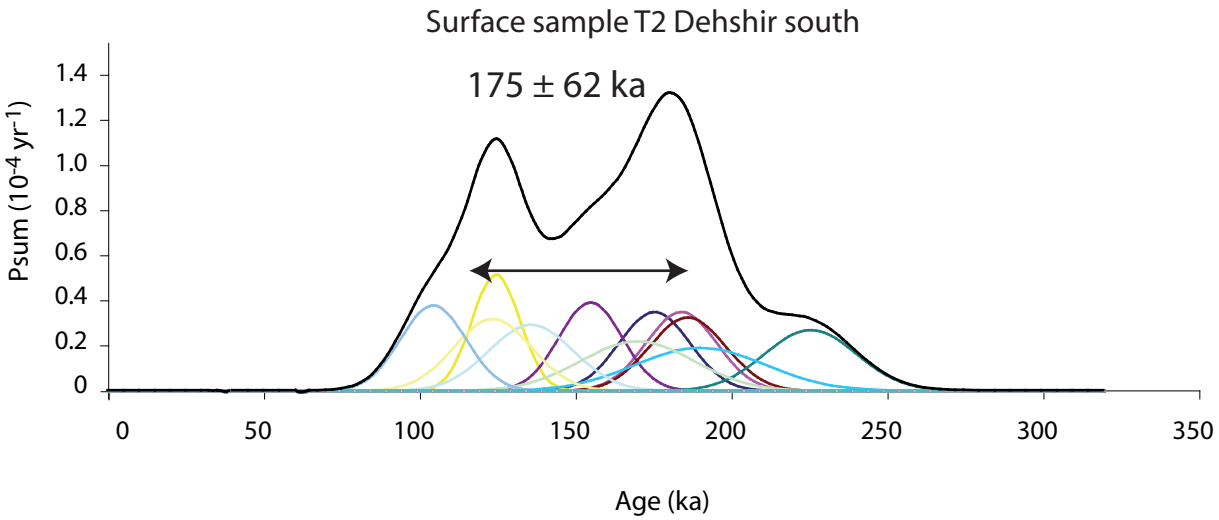


b)

c)

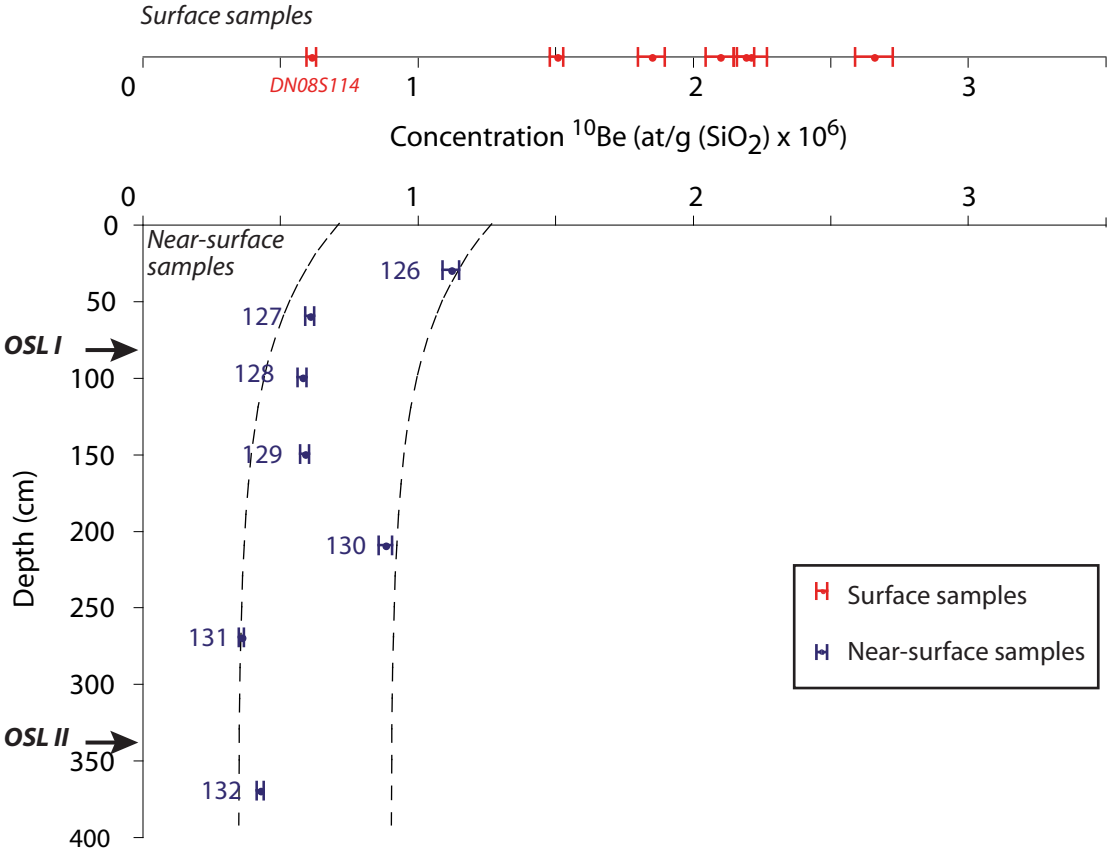

Figure 12

Profile PS2, Dehshir south T2

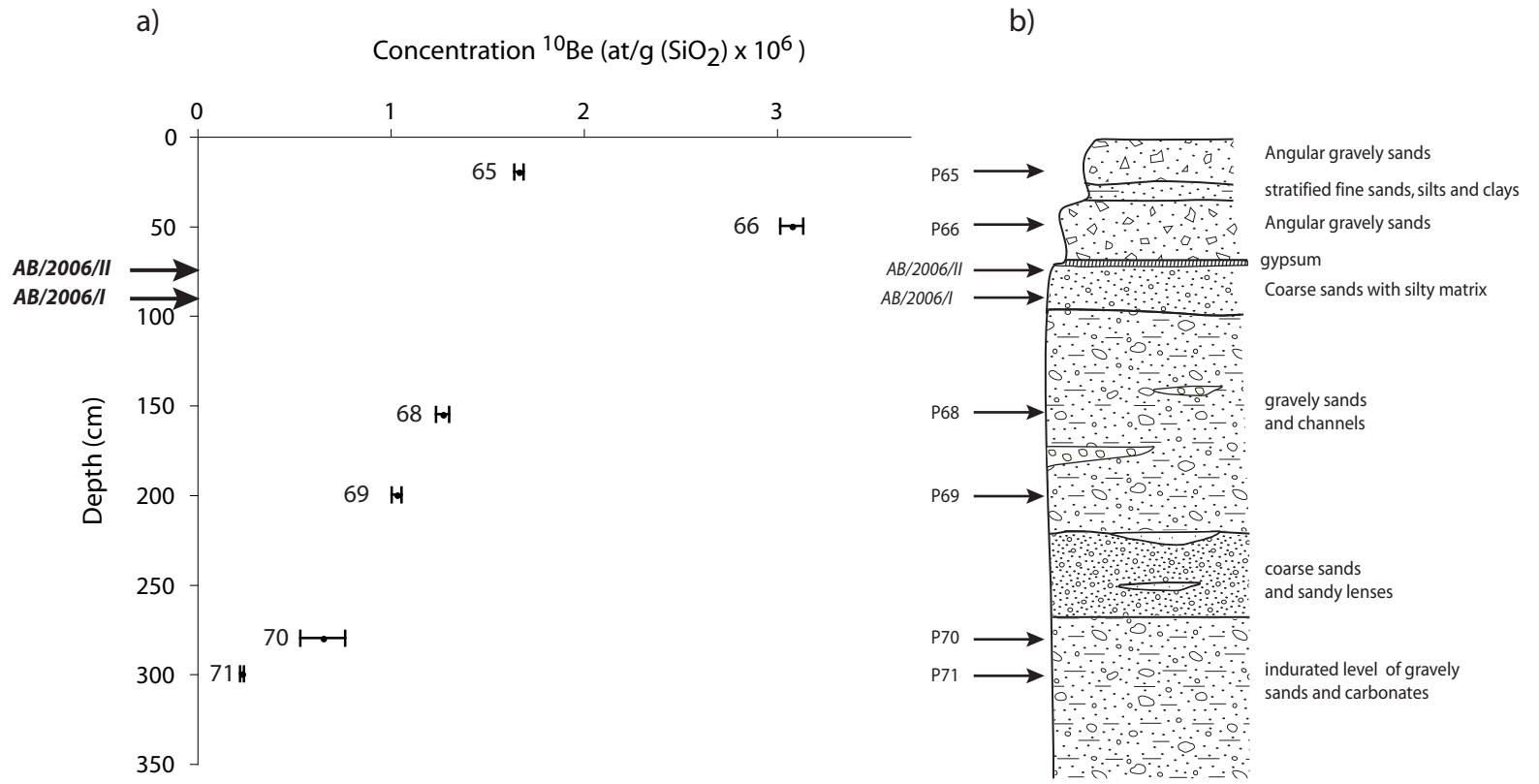

Figure 13

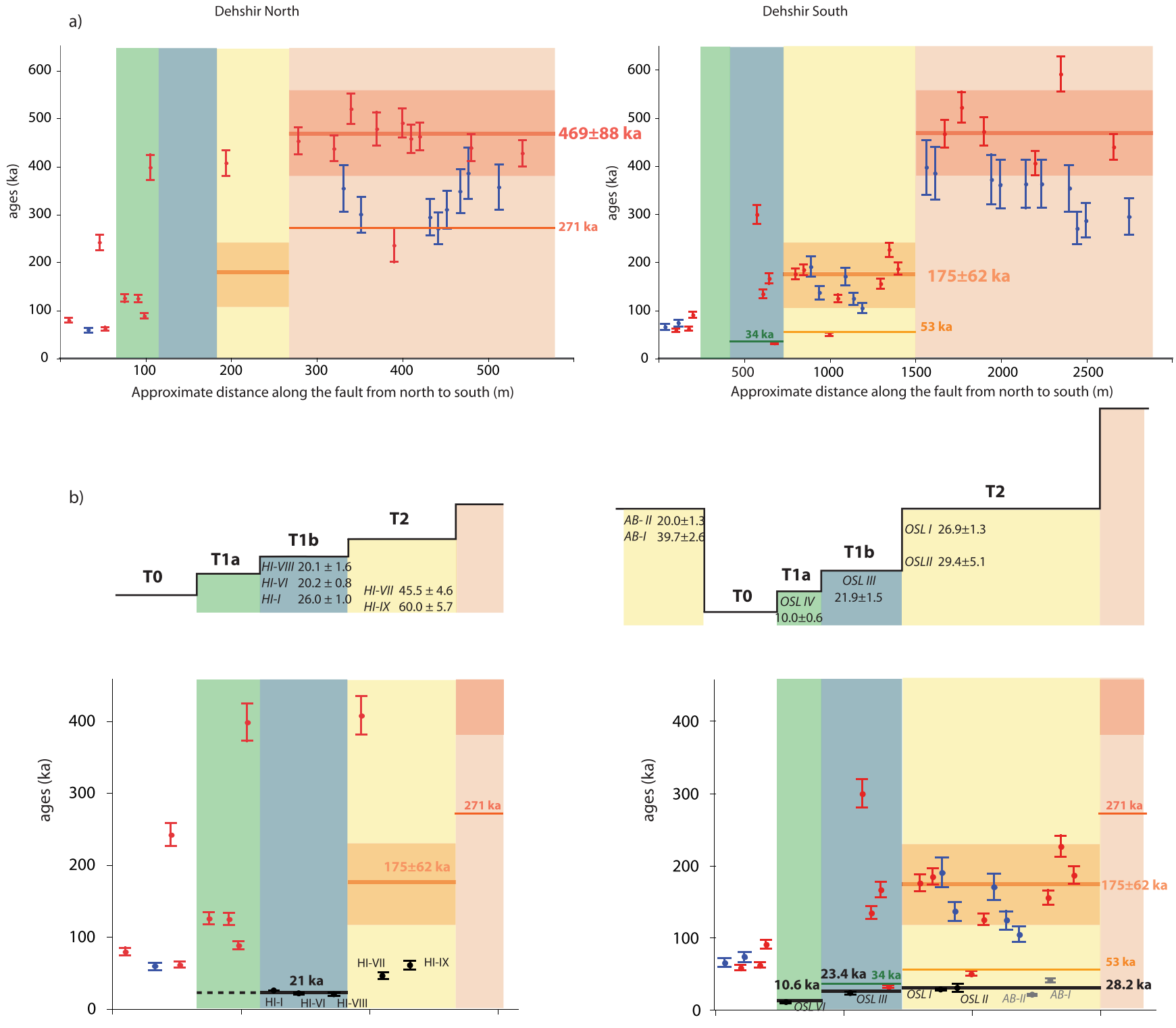
a)
Dehshir North
Dehshir South
ages (ka)
Approximate distance along the fault from north to south (m)
469±88 ka
271 ka
175±62 ka
53 ka
34 ka
b)
T0
T1a
T1b
T2
HI-VIII 20.1 ± 1.6
HI-VI 20.2 ± 0.8
HI-I 26.0 ± 1.0
HI-VII 45.5 ± 4.6
HI-IX 60.0 ± 5.7
AB- II 20.0±1.3
AB-I 39.7±2.6
OSL IV 10.0±0.6
OSL III 21.9±1.5
OSL I 26.9±1.3
OSLII 29.4±5.1
21 ka
HI-I
HI-VI
HI-VIII
HI-VII
HI-IX
10.6 ka
23.4 ka
34 ka
28.2 ka
OSL VI
OSL III
OSL I
OSL II
AB-II
AB-I

Figure 14

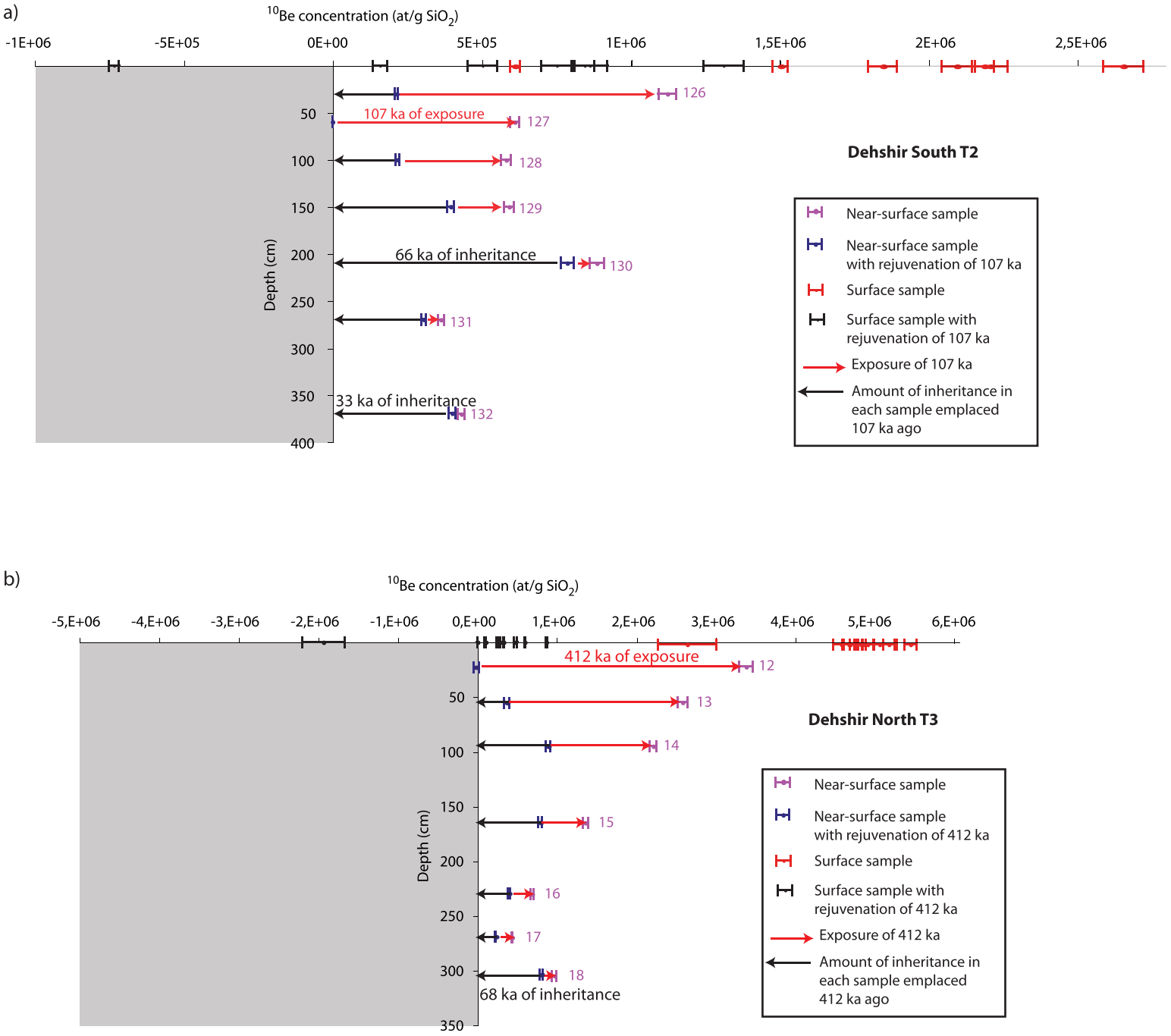
a)
$^{10}$Be concentration (at/g SiO$_2$)
-1E+06
-5E+05
0E+00
5E+05
1E+06
1,5E+06
2E+06
2,5E+06
Depth (cm)
50
100
150
200
250
300
350
400
126
107 ka of exposure
127
128
129
66 ka of inheritance
130
131
33 ka of inheritance
132
Dehshir South T2
Near-surface sample
Near-surface sample with rejuvenation of 107 ka
Surface sample
Surface sample with rejuvenation of 107 ka
Exposure of 107 ka
Amount of inheritance in each sample emplaced 107 ka ago
b)
$^{10}$Be concentration (at/g SiO$_2$)
-5,E+06
-4,E+06
-3,E+06
-2,E+06
-1,E+06
0,E+00
1,E+06
2,E+06
3,E+06
4,E+06
5,E+06
6,E+06
Depth (cm)
50
100
150
200
250
300
350
412 ka of exposure
12
13
14
15
16
17
18
68 ka of inheritance
Dehshir North T3
Near-surface sample
Near-surface sample with rejuvenation of 412 ka
Surface sample
Surface sample with rejuvenation of 412 ka
Exposure of 412 ka
Amount of inheritance in each sample emplaced 412 ka ago

Figure 15

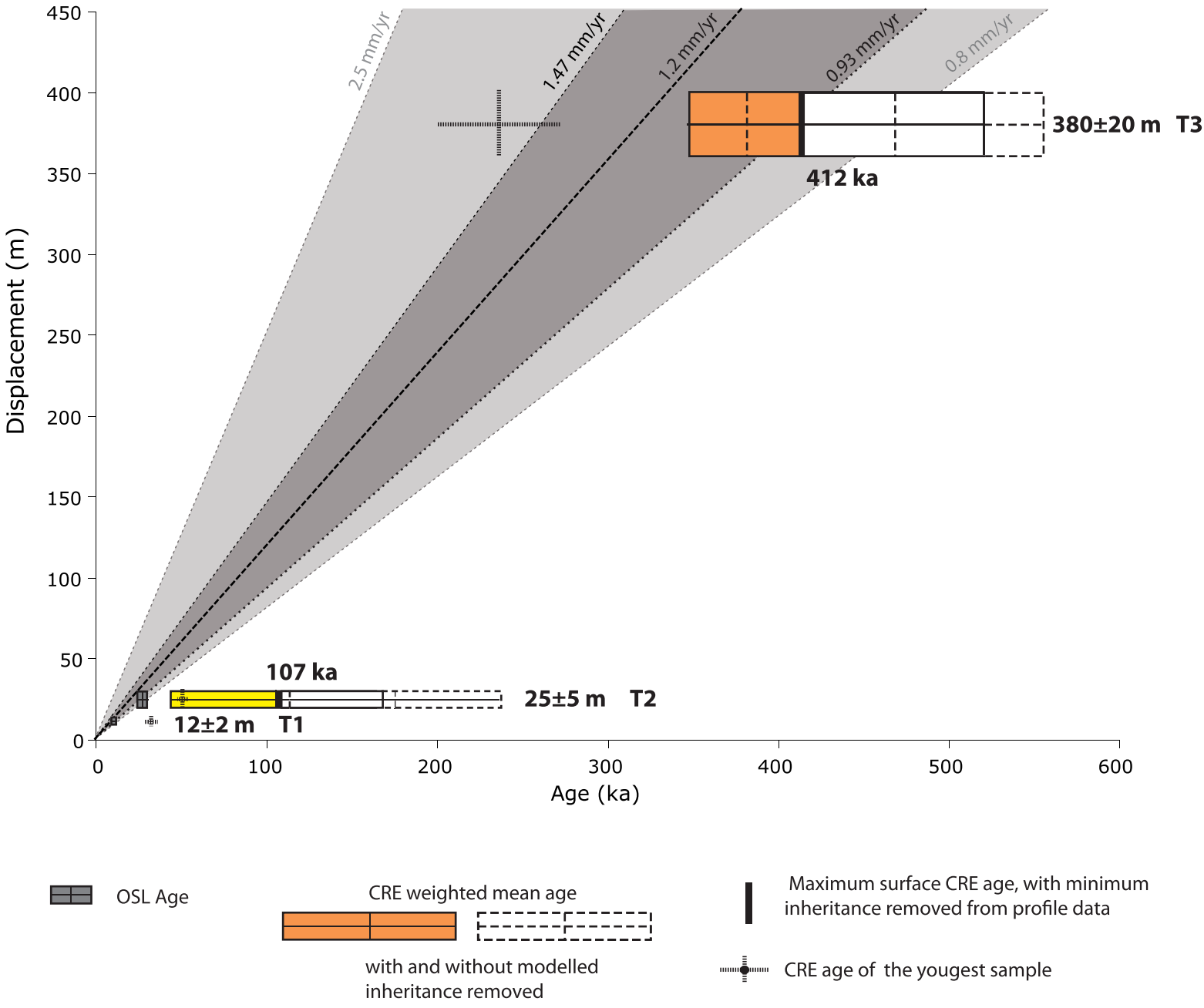
Displacement (m)
Age (ka)
2.5 mm/yr
1.47 mm/yr
1.2 mm/yr
0.93 mm/yr
0.8 mm/yr
380±20 m T3
412 ka
107 ka
25±5 m T2
12±2 m T1
OSL Age
CRE weighted mean age
with and without modelled inheritance removed
Maximum surface CRE age, with minimum inheritance removed from profile data
CRE age of the yougest sample

| | | | | | | | $^{10}$Be | | | | $^{36}$Cl | | | |
|---|---|---|---|---|---|---|---|---|---|---|---|---|---|---|
| **Samples** | **Sample description** | **Density (g.cm$^{-3}$)** | **Thickness (cm)** | **Latitude (°N)** | **Longitude (°E)** | **Elevation (m)** | **Stone scaling factor** | **Measured $^{10}$Be ($10^5$ at.g$^{-1}$SiO2)** | **$^{10}$Be model age (ka) no erosion** | **$^{10}$Be maximum erosion rate (m.Ma$^{-1}$)** | **Cl (ppm)** | **Measured $^{36}$Cl ($10^7$ at.g$^{-1}$ rock)** | **$^{36}$Cl model age (ka) no erosion** | **$^{36}$Cl maximur erosion rate (m.Ma$^{-1}$)** |
| **Dehshir North** | | | | | | | | | | | | | | |
| **T0** | | | | | | | | | | | | | | |
| DN06S30 | cobble (15 cm) in the river bed | 2.2 | 6 | 30.6457 | 54.0236 | 1539 | 2.64 | 9.23±0.22 | 79.42±5.14 | 8.98 | | | | |
| DN08S120 | cobble (10 cm) in the river bed | 2.2 | 8 | 30.64414 | 54.02172 | 1548 | 2.65 | 27.16±0.71 | 241.55±15.80 | 3.16 | | | | |
| DN08S121 | cobble (15 cm) in the river bed | 2.2 | 7 | 30.64111 | 54.01947 | 1547 | 2.65 | 7.18±0.19 | 61.15±4.03 | 14.30 | | | | |
| DN06S29 | cobble (15 cm) in the river bed | 2 | 7 | 30.64571 | 54.02366 | 1539 | | | | | 52 | 0.32±0.005 | 56.40±5.16 | 17.16 |
| **T1** | | | | | | | | | | | | | | |
| DN08S115 | cobble (10 cm) | 2.2 | 6 | 30.64343 | 54.02151 | 1550 | 2.66 | 43.06±1.17 | 397.28±26.16 | 1.79 | | | | |
| DN08S116 | cobble (10 cm) | 2.2 | 6 | 30.64351 | 54.02167 | 1549 | 2.65 | 10.30±0.28 | 88.19±5.81 | 9.62 | | | | |
| DN08S117 | cobble (10 cm) | 2.2 | 7 | 30.64355 | 54.0218 | 1550 | 2.66 | 14.42±0.39 | 124.44±8.19 | 6.60 | | | | |
| DN08S118 | cobble (15 cm) | 2.2 | 6 | 30.64362 | 54.02177 | 1549 | 2.65 | 14.55±0.39 | 125.69±8.26 | 6.53 | | | | |
| **T2** | | | | | | | | | | | | | | |
| DN08A119 | Amalgam (25 pluricentimetric clasts) | 2.2 | - | 30.64337 | 54.02239 | 1550 | 2.66 | 43.97±1.11 | 406.54±26.47 | 1.74 | | | | |
| **T3** | | | | | | | | | | | | | | |
| DN06S1 | cobble (10 cm) | 2.2 | 3 | 30.64068 | 54.01913 | 1550 | 2.72 | N.M | - | - | | | | |
| DN06S2 | 2 fragments of the same gelyfracted cobble | 2.2 | 3 | 30.64065 | 54.01907 | 1550 | 2.66 | 26.55±3.66 | 235.55±35.38 | 2.91 | | | | |
| DN06S6 | cobble (10 cm) | 2.2 | 5 | 30.640361 | 54.021083 | 1550 | 2.66 | 51.88±0.72 | 489.51±30.15 | 1.31 | | | | |
| DN06S7 | cobble (15 cm) | 2.2 | 4 | 30.64045 | 54.02092 | 1550 | 2.66 | 48.78±1.19 | 456.66±29.58 | 1.42 | | | | |
| DN06S10 | cobble (10 cm) | 2.2 | 5 | 30.6405 | 54.020917 | 1550 | 2.66 | 49.21±0.69 | 461.15±28.42 | 1.40 | | | | |
| DN06A11 | Amalgam (20 pluricentimetric clasts) | 2.2 | - | 30.6405 | 54.020917 | 1550 | 2.66 | 48.37±0.66 | 452.25±27.83 | 1.43 | | | | |
| DN06S19 | cobble (10 cm) | 2.2 | 4 | 30.64208 | 54.02502 | 1550 | 2.66 | 46.84±0.65 | 436.33±26.88 | 1.49 | | | | |
| DN06S21 | cobble (10 cm) | 2.2 | 4 | 30.64189 | 54.02503 | 1550 | 2.66 | 54.60±0.75 | 518.71±31.93 | 1.23 | | | | |
| DN06S23 | cobble (10 cm) | 2.2 | 7 | 30.64177 | 54.0251 | 1550 | 2.66 | 50.72±2.12 | 477.09±34.88 | 1.35 | | | | |
| DN06S26 | cobble (10 cm) | 2.2 | 8 | 30.64101 | 54.02506 | 1550 | 2.66 | 46.99±1.02 | 437.88±27.94 | 1.49 | | | | |
| DN06S28 | cobble (20 cm) | 2.2 | 9 | 30.64038 | 54.02512 | 1550 | 2.66 | 45.92±0.99 | 426.74±27.23 | 1.53 | | | | |
| DN06S3 | cobble (10 cm) | 2 | 8 | 30.640417 | 54.021222 | 1554 | | | | | 16 | 1.21±0.011 | 291.88±37.60 | 1.80 |
| DN06S4 | cobble (10 cm) | 2 | 5 | 30.640333 | 54.021083 | 1556 | | | | | 18 | 1.18±0.014 | 268.43±33.33 | 2.10 |
| DNS06S5 | 2 fragments of the same gelyfracted cobble | 2 | 4 | 30.640333 | 54.021083 | 1556 | | | | | 26 | N.M | - | - |
| DNS06S8 | cobble (15 cm) | 2 | 3 | 30.640389 | 54.021055 | 1555 | | | | | 28 | N.M | - | - |
| DNS06S9 | cobble (10 cm) | 2 | 5 | 30.640361 | 54.020972 | 1552 | | | | | 13 | 1.30±0.018 | 351.98±48.07 | 1.33 |
| DN06S20 | cobble (10 cm) | 2 | 5 | 30.64208 | 54.02504 | 1550 | | | | | 24 | 1.36±0.013 | 345.97±45.90 | 1.48 |
| DN06S22 | cobble (10 cm) | 2 | 3 | 30.64189 | 54.0251 | 1550 | | | | | 19 | 1.25±0.019 | 297.22±37.59 | 1.79 |
| DN06S24 | cobble (10 cm) | 2 | 3 | 30.64129 | 54.02508 | 1549 | | | | | 18 | 1.31±0.014 | 307.95±39.30 | 1.68 |
| DN06S25 | cobble (10 cm) | 2 | 3 | 30.64108 | 54.02507 | 1550 | | | | | 40 | 1.53±0.024 | 383,59±53.46 | 1.40 |
| DN06S27 | cobble (10 cm) | 2 | 4 | 30.64099 | 54.02521 | 1550 | | | | | 38 | 1.41±0.02 | 354.70±47.24 | 1.57 |

| | | | | | | | $^{10}$Be | | | | $^{36}$Cl | | | |
|---|---|---|---|---|---|---|---|---|---|---|---|---|---|---|
| **Samples** | **Sample description** | **Density (g.cm$^{-3}$)** | **Thickness (cm)** | **Latitude (°N)** | **Longitude (°E)** | **Elevation (m)** | **Stone scaling factor** | **Measured $^{10}$Be ($10^5$ at.g$^{-1}$SiO2)** | **$^{10}$Be model age (ka) no erosion** | **$^{10}$Be maximum erosion rate (m.Ma$^{-1}$)** | **Cl (ppm)** | **Measured $^{36}$Cl ($10^7$ at.g$^{-1}$ rock)** | **$^{36}$Cl model age (ka). no erosion** | **$^{36}$Cl maximum erosion rate (m.Ma$^{-1}$)** |
| **Dehshir South** | | | | | | | | | | | | | | |
| **T0** | | | | | | | | | | | | | | |
| DS06S64 | cobble (15 cm) in the river bed | 2.2 | 7 | 30.44864 | 54.12418 | 1620 | 2.77 | 7.11±0.15 | 57.78±3.68 | 12.41 | | | | |
| DS08S109 | cobble (15 cm) in the river bed | 2.2 | 5 | 30.44742 | 54.11986 | 1626 | 2.79 | 7.63±0.21 | 61.83±4.08 | 14.13 | | | | |
| DS08S110 | cobble (15 cm) in the river bed | 2.2 | 6 | 30.44926 | 54.13 | 1613 | 2.76 | 10.97±0.29 | 90.34±5.94 | 9.37 | | | | |
| DS06S62 | cobble (10 cm) in the river bed | 2 | 4 | 30.44866 | 54.12527 | 1615 | | | | | 60 | 0.45±0.007 | 72.83±6.82 | 12.94 |
| DN06S63 | cobble (10 cm) in the river bed | 2 | 5 | 30.44881 | 54.12454 | 1615 | | | | | 52 | 0.40±0.012 | 65.04±6.54 | 14.45 |
| **T1** | | | | | | | | | | | | | | |
| DS08S122 | cobble (10 cm) | 2.2 | 4 | 30.44743 | 54.12096 | 1626 | 2.79 | 34.77±0.93 | 298.60±19.60 | 2.48 | | | | |
| DS08S123 | cobble (15 cm) | 2.2 | 7 | 30.44741 | 54.12083 | 1626 | 2.79 | 19.96±0.52 | 165.94±10.87 | 4.80 | | | | |
| DS08S124 | cobble (10 cm) | 2.2 | 6 | 30.44716 | 54.12017 | 1627 | 2.79 | 3.99±0.11 | 32.07±2.12 | 28 .42 | | | | |
| DS08S125 | cobble (15 cm) | 2.2 | 6 | 30.44695 | 54.11975 | 1627 | 2.79 | 16.28±0.44 | 134.22±8.83 | 6.07 | | | | |
| **T2** | | | | | | | | | | | | | | |
| DS06S31 | cobble (10 cm) | 2.2 | 4 | 30.4476 | 54.12655 | 1622 | 2.78 | N.M | - | - | | | | |
| DS06S32 | cobble (10 cm) | 2.2 | 5 | 30.4476 | 54.12655 | 1622 | 2.78 | 21.01±0.52 | 175.57±11.39 | 3.96 | | | | |
| DS06S34 | cobble (20 cm) | 2.2 | 6 | 30.44765 | 54.12751 | 1619 | 2.77 | 21.95±0.32 | 184.19±11.38 | 3.77 | | | | |
| DS06S36 | cobble (20 cm) | 2.2 | 6 | 30.447 | 54.1284 | 1620 | 2.77 | 15.08±0.24 | 124.58±7.73 | 5.66 | | | | |
| DS06S40 | cobble (10 cm) | 2.2 | 5 | 30.44663 | 54.12945 | 1620 | 2.77 | N.M | - | - | | | | |
| DS08S111 | cobble (10 cm) | 2.2 | 6 | 30.44792 | 54.13517 | 1612 | 2.76 | 18.52±0.49 | 154.99±10.15 | 5.18 | | | | |
| DS08S112 | cobble (10 cm) | 2.2 | 7 | 30.44793 | 54.13371 | 1615 | 2.76 | 22.12±0.60 | 186.22±12.26 | 4.22 | | | | |
| DS08S113 | cobble (10 cm) | 2.2 | 7 | 30.44708 | 54.13213 | 1618 | 2.77 | 26.61±0.68 | 225.76±14.73 | 3.41 | | | | |
| DS08S114 | cobble (10 cm) | 2.2 | 6 | 30.44803 | 54.13074 | 1623 | 2.78 | 6.16±0.17 | 49.87±3.29 | 17.80 | | | | |
| DS06S33 | cobble (15 cm) | 2 | 7 | 30.44759 | 54.1265 | 1620 | | | | | 24 | 0.97±0.009 | 190.26±20.80 | 3.38 |
| DS06S35 | cobble (20 cm) | 2 | 5 | 30.44764 | 54.12754 | 1621 | | | | | 52 | 0.76±0.009 | 135.85±13.57 | 6.01 |
| DS06S37 | cobble (10 cm) | 2 | 4 | 30.44695 | 54.1284 | 1620 | | | | | 23 | 0.87±0.009 | 170.02±18.11 | 3.92 |
| DS06S38 | cobble (10 cm) | 2 | 4 | 30.44669 | 54.12885 | 1615 | | | | | 43 | 0.67±0.098 | 123.50±12.49 | 6.50 |
| DS06S39 | cobble (10 cm) | 2 | 4 | 30.44663 | 54.12946 | 1620 | | | | | 11 | 0.57±0.009 | 104.41±10.51 | 6.89 |
| **T3** | | | | | | | | | | | | | | |
| DS06S41 | 2 fragments of the same gelyfracted cobble | 2.2 | 6 | 30.4408 | 54.11883 | 1632 | 2.80 | 52.28±0.75 | 465.68±28.72 | 1.39 | | | | |
| DS06S44 | cobble (15 cm) | 2.2 | 8 | 30.43993 | 54.11873 | 1636 | 2.80 | 57.81±0.81 | 520.28±32.06 | 1.22 | | | | |
| DS06S45 | cobble (15 cm) | 2.2 | 5 | 30.43552 | 54.12536 | 1632 | 2.80 | 52.76±0.84 | 470.58±29.21 | 1.37 | | | | |
| DS06S48 | cobble (15 cm) | 2.2 | 8 | 30.43532 | 54.12533 | 1630 | 2.79 | N.M | - | - | | | | |
| DS06S49 | cobble (20 cm) | 2.2 | 9 | 30.43518 | 54.1263 | 1630 | 2.79 | N.M | - | - | | | | |
| DS06S51 | 2 fragments of the same gelyfracted cobble | 2.2 | 6 | 30.43475 | 54.13594 | 1620 | 2.77 | N.M | - | - | | | | |
| DS06S53 | cobble (10 cm) | 2.2 | 5 | 30.43517 | 54.13687 | 1623 | 2.78 | 49.22±0.66 | 438.32±26.95 | 1.48 | | | | |
| DS06S54 | cobble (15 cm) | 2.2 | 6 | 30.43521 | 54.13694 | 1618 | 2.77 | N.M | - | - | | | | |
| DS06S56 | cobble (10 cm) | 2.2 | 8 | 30.4369 | 54.138 | 1620 | 2.77 | 63.71±0.90 | 589.48±36.34 | 1.06 | | | | |
| DS06S60 | cobble (15 cm) | 2.2 | 7 | 30.43971 | 54.13797 | 1620 | 2.77 | 45.77±0.65 | 405.18±24.98 | 1.62 | | | | |
| DS06S42 | 1 fragment of a gelyfracted cobble (15 cm) | 2 | 5 | 30.4407 | 54.11863 | 1630 | | | | | 17 | 1.51±0.022 | 384.20±54.50 | 1.19 |
| DS06S43 | cobble (15 cm) | 2 | 4 | 30.44082 | 54.11877 | 1632 | | | | | 17 | 1.55±0.015 | 396.25±56.62 | 1.13 |
| DS06S46 | cobble (10 cm) | 2 | 3 | 30.43548 | 54.12536 | 1630 | | | | | 14 | 1.54±0.014 | 371.29±52.05 | 1.21 |
| DS06S47 | cobble (15 cm) | 2 | 6 | 30.43538 | 54.12553 | 1630 | | | | | 26 | 1.46±0.034 | 361.52±50.52 | 1.40 |
| DS06S50 | cobble (15 cm) | 2 | 4 | 30.4351 | 54.12631 | 1631 | | | | | 18 | 1.45±0.016 | 363.29±49.85 | 1.03 |
| DS06S52 | cobble (10 cm) | 2 | 4 | 30.43482 | 54.13612 | 1625 | | | | | 16 | 1.24±0.014 | 287.11±35.74 | 1.84 |
| DS06S55 | cobble (15 cm) | 2 | 5 | 30.43515 | 54.13692 | 1626 | | | | | 17 | 1.27±0.020 | 294.57±37.25 | 1.79 |
| DS06S57 | cobble (10 cm) | 2 | 5 | 30.43708 | 54.13814 | 1627 | | | | | 10 | 1.44±0.013 | 352.98±48.02 | 1.29 |
| DS06S58 | cobble (15 cm) | 2 | 8 | 30.43708 | 54.13814 | 1627 | | | | | 10 | 1.19±0.023 | 271.00±33.83 | 1.92 |
| DS06S59 | cobble (10 cm) | 2 | 6 | 30.43941 | 54.13816 | 1625 | | | | | 8 | 1.41±0.011 | 362.38±49.94 | 1.22 |

| | | | | | | | $^{10}$Be | | | | $^{36}$Cl | | | |
|---|---|---|---|---|---|---|---|---|---|---|---|---|---|---|
| **Samples** | **Sample description** | **Density (g.cm$^{-3}$)** | **Thickness (cm)** | **Latitude (°N)** | **Longitude (°E)** | **Elevation (m)** | **Stone scaling factor** | **Measured $^{10}$Be ($10^5$ at.g$^{-1}$SiO2)** | **$^{10}$Be model age (ka) no erosion** | **$^{10}$Be maximum erosion rate (m.Ma$^{-1}$)** | **Cl (ppm)** | **Measured $^{36}$Cl ($10^7$ at.g$^{-1}$ rock)** | **$^{36}$Cl model age (ka). no erosion** | **$^{36}$Cl maximur erosion rate (m.Ma$^{-1}$)** |
| **Dehshir North $^{10}$Be** | | | | | | | | | | | | | | |
| **Pit in the surface T3 PN[a]** | | | | | | 1550 | | | | | | | | |
| DN06P12Q | amalgam 25 cm below ground surface | 2.2 | - | 30.64114 | 54.02133 | | 2.66 | 33.77±0.85 | | | | | | |
| DN06P13Q | amalgam 55 cm below ground surface | 2.2 | - | 30.64114 | 54.02133 | | 2.66 | 25.80±0.66 | | | | | | |
| DN06P14Q | amalgam 95 cm below ground surface | 2.2 | - | 30.64114 | 54.02133 | | 2.66 | 22.12±0.45 | | | | | | |
| DN06P15Q | amalgam 165 cm below ground surface | 2.2 | - | 30.64114 | 54.02133 | | 2.66 | 13.60±0.34 | | | | | | |
| DN06P16Q | amalgam 230 cm below ground surface | 2.2 | - | 30.64114 | 54.02133 | | 2.66 | 6.89±0.17 | | | | | | |
| DN06P17Q | amalgam 270 cm below ground surface | 2.2 | - | 30.64114 | 54.02133 | | 2.66 | 4.37±0.07 | | | | | | |
| DN06P18Q | amalgam 305 cm below ground surface | 2.2 | - | 30.64114 | 54.02133 | | 2.66 | 9.68±0.24 | | | | | | |
| **Dehshir North $^{36}$Cl [a]** | | | | | | | | | | | | | | |
| **Pit in the surface T3** | | | | | | 1550 | | | | | | | | |
| DN06P12C | amalgam 25 cm below ground surface | 2.2 | - | 30.64114 | 54.02133 | | | | | | 29 | 1.78±0.018 | | |
| DN06P13C | amalgam 55 cm below ground surface | 2.2 | - | 30.64114 | 54.02133 | | | | | | 32 | 1.30±0.015 | | |
| DN06P14C | amalgam 95 cm below ground surface | 2.2 | - | 30.64114 | 54.02133 | | | | | | 20 | 1.10±0.011 | | |
| DN06P15C | amalgam 165 cm below ground surface | 2.2 | - | 30.64114 | 54.02133 | | | | | | 38 | 0.63±0.024 | | |
| DN06P16C | amalgam 230 cm below ground surface | 2.2 | - | 30.64114 | 54.02133 | | | | | | 26 | 0.34±0.007 | | |
| DN06P18C | amalgam 305 cm below ground surface | 2.2 | - | 30.64114 | 54.02133 | | | | | | 22 | 0.18±0.004 | | |
| **Dehshir South $^{10}$Be** | | | | | | | | | | | | | | |
| **Riser T2/T0 PS1 [b]** | | | | | | 1645 | | | | | | | | |
| DS08P126 | amalgam 30 cm below ground surface | 2.2 | - | 30.44823 | 54.12648 | | 2.82 | 11.23±0.30 | | | | | | |
| DS08P127 | amalgam 60 cm below ground surface | 2.2 | - | 30.44823 | 54.12648 | | 2.82 | 6.10±0.17 | | | | | | |
| DS08P128 | amalgam 100 cm below ground surface | 2.2 | - | 30.44823 | 54.12648 | | 2.82 | 5.82±0.16 | | | | | | |
| DS08P129 | amalgam 150 cm below ground surface | 2.2 | - | 30.44823 | 54.12648 | | 2.82 | 5.91±0.16 | | | | | | |
| DS08P130 | amalgam 210 cm below ground surface | 2.2 | - | 30.44823 | 54.12648 | | 2.82 | 8.86±0.24 | | | | | | |
| DS08P131 | amalgam 270 cm below ground surface | 2.2 | - | 30.44823 | 54.12648 | | 2.82 | 3.62±0.10 | | | | | | |
| DS08P132 | amalgam 370 cm below ground surface | 2.2 | - | 30.44823 | 54.12648 | | 2.82 | 4.31±0.12 | | | | | | |
| **Pit in the surface T2 PS2 [a]** | | | | | | 1628 | | | | | | | | |
| DS06P65 | amalgam 20 cm below ground surface | 2.2 | - | 30.45705 | 54.11839 | | 2.79 | 16.67±0.24 | | | | | | |
| DS06P66 | amalgam 50 cm below ground surface | 2.2 | - | 30.45705 | 54.11839 | | 2.79 | 30.80±0.60 | | | | | | |
| DS06P67 | amalgam 80 cm below ground surface | 2.2 | - | 30.45705 | 54.11839 | | 2.79 | N.M | | | | | | |
| DS06P68 | amalgam 155 cm below ground surface | 2.2 | - | 30.45705 | 54.11839 | | 2.79 | 12.72±0.33 | | | | | | |
| DS06P69 | amalgam 200 cm below ground surface | 2.2 | - | 30.45705 | 54.11839 | | 2.79 | 10.33±0.25 | | | | | | |
| DS06P70 | amalgam 280 cm below ground surface | 2.2 | - | 30.45705 | 54.11839 | | 2.79 | 6.51±1.17 | | | | | | |
| DS06P71 | amalgam 300 cm below ground surface | 2.2 | - | 30.45705 | 54.11839 | | 2.79 | 2.32±0.10 | | | | | | |

| Samples | $H_2O$ % | $Al_2O_3$ % | CaO % | $Fe_2O_3$ % | $K_2O$ % | MgO % | MnO % | $Na_2O$ % | $P_2O_5$ % | $SiO_2$ % | $TiO_2$ % | Th % | U % |
|---|---|---|---|---|---|---|---|---|---|---|---|---|---|
| DN06S3 | 0.30 | 0.04 | 54.38 | 0.15 | 0 | 0.59 | 0.01 | 0 | 0.02 | 0.11 | 0.00 | 0.020 | 0.763 |
| DN06S4 | 0.35 | 0.15 | 53.85 | 0.08 | 0 | 0.90 | 0.02 | 0 | 0.02 | 0.21 | 0.01 | 0.113 | 2.740 |
| DN06S5 | 0.29 | 0.09 | 54.39 | 0.10 | 0 | 0.68 | 0.01 | 0 | 0.02 | 0.11 | 0.00 | 0.064 | 1.295 |
| DN06S8 | 0.22 | 0.07 | 54.92 | 0.08 | 0 | 0.57 | 0.01 | 0 | 0.02 | 0.00 | 0.01 | 0.058 | 0.382 |
| DNS06S9 | 0.29 | 0.09 | 54.39 | 0.10 | 0 | 0.68 | 0.01 | 0 | 0.02 | 0.11 | 0.00 | 0.064 | 1.295 |
| DN06P12C | 0.41 | 0.40 | 52.75 | 0.33 | 0.09 | 0.92 | 0.02 | 0 | 0 | 1.99 | 0.03 | 0.309 | 1.164 |
| DN06P13 | 0.41 | 0.40 | 52.75 | 0.33 | 0.09 | 0.92 | 0.02 | 0 | 0 | 1.99 | 0.03 | 0.309 | 1.164 |
| DN06P14C | 0.41 | 0.40 | 52.75 | 0.33 | 0.09 | 0.92 | 0.02 | 0 | 0 | 1.99 | 0.03 | 0.309 | 1.164 |
| DN06P15C | 0.41 | 0.40 | 52.75 | 0.33 | 0.09 | 0.92 | 0.02 | 0 | 0 | 1.99 | 0.03 | 0.309 | 1.164 |
| DN06P16C | 0.41 | 0.40 | 52.75 | 0.33 | 0.09 | 0.92 | 0.02 | 0 | 0 | 1.99 | 0.03 | 0.309 | 1.164 |
| DN06P18C | 0.41 | 0.40 | 52.75 | 0.33 | 0.09 | 0.92 | 0.02 | 0 | 0 | 1.99 | 0.03 | 0.309 | 1.164 |
| DNO6S20 | 0.31 | 0.08 | 53.74 | 0.15 | 0 | 1.20 | 0.03 | 0 | 0 | 0.12 | 0.00 | 0.048 | 0.861 |
| DN06S22 | 0.26 | 0.02 | 54.28 | 0.04 | 0 | 1.10 | 0.00 | 0 | 0 | 0.00 | 0.00 | 0.000 | 1.330 |
| DNO6S24 | 0.31 | 0.08 | 53.74 | 0.15 | 0 | 1.20 | 0.03 | 0 | 0 | 0.12 | 0.00 | 0.048 | 0.861 |
| DN06S25 | 0.36 | 0.14 | 53.20 | 0.26 | 0 | 1.31 | 0.05 | 0 | 0 | 0.24 | 0.01 | 0.095 | 0.392 |
| DNO6S27 | 0.31 | 0.08 | 53.74 | 0.15 | 0 | 1.20 | 0.03 | 0 | 0 | 0.12 | 0.00 | 0.048 | 0.861 |
| DNO6S29 | 0.31 | 0.08 | 53.74 | 0.15 | 0.00 | 1.20 | 0.03 | 0 | 0.00 | 0.12 | 0.00 | 0.048 | 0.861 |
| DS06S33 | 0.245 | 0.022 | 54.39 | 0.06 | 0 | 0.652 | 0.0035 | 0 | 0.008 | 0 | 0 | 0.025 | 1.433 |
| DS06S35 | 0.245 | 0.022 | 54.39 | 0.06 | 0 | 0.652 | 0.0035 | 0 | 0.008 | 0 | 0 | 0.025 | 1.433 |
| DS06S37 | 0.245 | 0.022 | 54.39 | 0.06 | 0 | 0.652 | 0.0035 | 0 | 0.008 | 0 | 0 | 0.025 | 1.433 |
| DS06S38 | 0.27 | 0.02 | 54.08 | 0.05 | 0 | 0.87 | 0.01 | 0 | 0.02 | 0.00 | 0.00 | 0.028 | 0.370 |
| DS06S39 | 0.22 | 0.02 | 54.71 | 0.08 | 0 | 0.44 | 0.00 | 0 | 0.00 | 0.00 | 0.00 | 0.021 | 2.495 |
| DS06S42 | 0.27 | 0.05 | 54.89 | 0 | 0 | 0.55 | 0 | 0 | 0 | 0 | 0.00 | 0.096 | 3.010 |
| DSO6S43 | 0.27 | 0.05 | 54.89 | 0 | 0 | 0.55 | 0 | 0 | 0 | 0 | 0.00 | 0.096 | 3.010 |
| DS06S46 | 0.27 | 0.05 | 54.89 | 0 | 0 | 0.55 | 0 | 0 | 0 | 0 | 0.00 | 0.096 | 3.010 |
| DSO6S47 | 0.27 | 0.05 | 54.89 | 0 | 0 | 0.55 | 0 | 0 | 0 | 0 | 0.00 | 0.096 | 3.010 |
| DS06S50 | 0.27 | 0.05 | 54.89 | 0 | 0 | 0.55 | 0 | 0 | 0 | 0 | 0.00 | 0.096 | 3.010 |
| DNO6S52 | 0.28 | 0 | 54.60 | 0.12 | 0 | 0.38 | 0 | 0 | 0 | 0 | 0.00 | 0.020 | 2.995 |
| DSO6S55 | 0.28 | 0 | 54.60 | 0.12 | 0 | 0.38 | 0 | 0 | 0 | 0 | 0.00 | 0.020 | 2.995 |
| DS06S57 | 0.28 | 0 | 54.60 | 0.12 | 0 | 0.38 | 0 | 0 | 0 | 0 | 0.00 | 0.020 | 2.995 |
| DSO6S58 | 0.28 | 0 | 54.60 | 0.12 | 0 | 0.38 | 0 | 0 | 0 | 0 | 0.00 | 0.020 | 2.995 |
| DSO6S59 | 0.28 | 0 | 54.60 | 0.12 | 0 | 0.38 | 0 | 0 | 0 | 0 | 0.00 | 0.020 | 2.995 |
| DS06S62 | 0.22 | 0.04 | 54.16 | 0.16 | 0.00 | 0.90 | 0.03 | 0.00 | 0.00 | 0.00 | 0.00 | 0.045 | 0.675 |
| DS06S63 | 0.22 | 0.04 | 54.16 | 0.16 | 0.00 | 0.90 | 0.03 | 0.00 | 0.00 | 0.00 | 0.00 | 0.045 | 0.675 |

| Sample | Latitude (°N) | Longitude (°E) | Depth (m) | Water (%) | K (%) | U (%) | Th (%) | Equivalent Dose CAM (Gy) | Equivalent Dose FMM* (Gy) | Annual dose rate ($Gy.ka^{-1}$) | Age (ka) |
|---|---|---|---|---|---|---|---|---|---|---|---|
| **Site Dehshir North** | | | | | | | | | | | |
| **Trench (alluviums coeval with T1 aggradation)** | | | | | | | | | | | |
| HI/2006-VI | 30.64121 | 54.02127 | 1.5 | 1.3 | 1.27±0.01 | 2.04±0.05 | 6.0±0.1 | 48.8±0.3 | | 2.43±0.09 | 20.2±0.8 [c] |
| HI/2008-VIII | 30.64123 | 54.02148 | 0.95 | 0.9 | 0.66±0.01 | 1.13±0.05 | 4.6±0.1 | 45.3±7.1 | 29.3±2.0 | 1.45±0.03 | 20.1±1.6 [f] |
| HI/2006-I | 30.64118 | 54.02131 | 1.2 | 0.9 | 1.22±0.01 | 1.79±0.05 | 6.0±0.1 | 60.2±0.28 | | 2.29±0.09 | 26.0±1.0 [c] |
| **Trench (alluviums coeval with T2 aggradation)** | | | | | | | | | | | |
| HI/2008-VII | 30.64123 | 54.02145 | 1.6 | 1.1 | 0.61±0.01 | 1.1±0.05 | 4.3±0.1 | 62.0±6.0 | | 1.36±0.03 | 45.5±4.6 [c] |
| HI/2008-IX | 30.64123 | 54.02150 | 2.8 | 1.2 | 0.66±0.01 | 1.12±0.05 | 4.5±0.1 | 83.0±7.3 | | 1.40±0.03 | 60.0±5.7 [c] |
| **Site Dehshir South** | | | | | | | | | | | |
| **Riser T2/T0** | | | | | | | | | | | |
| OSL I | 30.44823 | 54.12632 | 0.8 | 1.1±0.2 | 0.78±0.01 | 1.52±0.05 | 4.8±0.1 | 46.5±1.4 | | 1.73±0.04 | 26.9±1.3 [c] |
| OSL II | 30.84823 | 54.12658 | 3.4 | 1.05±0.2 | 0.85±0.01 | 1.05±0.05 | 4.2±0.1 | 45.6±7.7 | | 1.55±0.04 | 29.4±5.1 [c] |
| **Riser T1b/T0** | | | | | | | | | | | |
| OSL III | 30.44132 | 54.10805 | 2.64 | 0.35±0.2 | 0.67±0.01 | 0.95±0.05 | 3.4±0.1 | 28.9±1.7 | | 1.32±0.04 | 21.9±1.5 [c] |
| **Riser T1a/T0** | | | | | | | | | | | |
| OSL IV | 30.44116 | 54.10173 | 0.8 | 0.2±0.2 | 0.71±0.01 | 1.15±0.05 | 5.0±0.1 | 23.4±2.6 | 15.7±0.8 | 1.57±0.04 | 10.0±0.6 [f] |
| **Pit in the surface T2** | | | | | | | | | | | |
| AB/2006-I | 30.45719 | 54.11822 | 0.9 | 1.1±0.2 | 0.86±0.01 | 1.78±0.05 | 4.2±0.1 | 73.3±3.7 | 72.9±3.8 | 1.83±0.05 | 39.7±2.6 [f] |
| AB/2006-II | 30.45719 | 54.11831 | 0.7 | 1.1±0.2 | 1.1±0.01 | 1.64±0.05 | 5.9±0.1 | 57.4±7.6 | 43.2±2.3 | 2.16±0.05 | 20.0±1.3 [f] |

* Finite Mixture Modelling (Roberts et al 2000) of replicate De values only undertaken where De distributions were multimodal, skewed and/or scattered (see text for details).
[c] Age based on De determined using Central age Model (CAM; Galbraith et al. 1999).
[f] Age based on De determined using Finite mixture Modeling (FMM; Roberts et al 2000).